The First Events in Photosynthesis: Electronic Coupling and Energy Transfer Dynamics in the Photosynthetic Reaction Center from *Rhodobacter sphaeroides*

David C. Arnett,[†,‡] C. C. Moser,[§] P. L. Dutton,[§] and N. F. Scherer*[,||,⊥]

Departments of Chemistry, Biochemistry and Biophysics and Johnson Foundation, University of Pennsylvania, Philadelphia, PA 19104-6323, and Department of Chemistry, the James Franck Institute, and the Institute for Physical-Biological Dynamics, University of Chicago, 5735 S. Ellis Ave., Chicago, Illinois 60637

Received: November 4, 1998

The rapid electronic state dynamics that occur prior to charge separation in the photosynthetic reaction center of *Rhodobacter sphaeroides* R-26 are investigated by "two-color" wavelength-resolved pump-probe and anisotropy measurements. A narrow band (40 fs duration transform limited) pump pulse is used to selectively excite reaction center pigments: the accessory bacteriochlorophyll (B), the upper excitonic state of the special pair (P_{y+}), or the lower excitonic state of the special pair (P_{y-}). Population dynamics are then measured with a 12 fs duration probe pulse across the entire Q_y absorption spectral region as a function of time, wavelength, and polarization. Excitation of either P_{y-} or B results in the formation of a distinct optical band at 825 nm exhibiting polarization characteristics consistent with those expected for P_{y+}; the band appears instantaneously upon excitation of P_{y-} with a negative anisotropy and appears somewhat delayed after excitation of B. The dynamics observed following direct excitation of the P_{y+} absorption band, that is identified to occur at 825 nm, suggests that internal conversion between the excitonic states of P is rapid, occurring with a 65 fs time constant. Excitation of the accessory BChl (i.e., populating the excited state, B*) provides a detailed answer for the mechanism of energy transfer within the bacterial reaction center. The process proceeds via a two-step mechanism, flowing sequentially from B* to P_{y+} to P_{y-} with time constants of 120 and 65 fs, respectively. These results follow from a kinetic model analysis of several pump-wavelength-dependent and polarization-dependent differential probe transmission transients that yield the first spectrum of P_{y+} at room temperature. The coherent excitonic dynamics of the special pair states, P_{y-} and P_{y+}, are measured and analyzed for coupling strengths and time scales for electronic dephasing and population relaxation. These results, in conjunction with a range of the transient transmission spectra, suggest that the initially excited state of the zeroth order chromophores, i.e., B* and P_{y+}, is delocalized at the earliest times, consistent with a supermolecular picture of the reaction center.

I. Introduction

The bacterial reaction center of *Rhodobacter sphaeroides* is a pigment−protein complex designed to convert optical excitation into the initial electron-transfer event in photosynthesis. The reaction center contains six chlorophyll-like pigments arranged with approximate C_2 symmetry. The relative arrangement of these pigments within the protein matrix is well-known,[1−3] consisting of two strongly interacting bacteriochlorophyll molecules known as the special pair (P), two accessory bacteriochlorophylls (B), and two bacteriopheophytins (H).[4,5] Following optical excitation of P, either directly or through energy transfer, an electron is transferred to H with a 3 ps time constant;[5−12] this process is facilitated by the spatially intermediate chromophore, B.

Recent electronic structure calculations treat the photosynthetic reaction center as a supermolecule,[13,14] with all of the chromophores excitonically coupled to some extent. It is commonly accepted that the two BChl molecules making up the special pair interact strongly. The excitonic coupling of the P_L and P_M bacteriochlorophyll monomers leads to two distinct bands corresponding to symmetric and antisymmetric combinations of the two monomer Q_y transitions. For *Rb. sphaeroides*, the lower excitonic state (antisymmetric combination termed P_{y-}) produces the strong, broad absorption near 870 nm. It is optical excitation of this state that results in the initial charge separation.[5−12] The near-IR absorption spectrum of the photosynthetic reaction center is shown in Figure 1. The absorption bands due to the Q_y transitions of the bacteriopheophytins (H) and accessory bacteriochlorophylls (B) are labeled, as are the two excitonic states of the special pair, P_{y-} at 865 nm and P_{y+} in the region of 810 nm to 825 nm. The upper excitonic state, P_{y+}, has proven to be more problematic to characterize than P_{y-}, with the orientation, extinction coefficient, and energy of this state being well established only at low temperatures; the most reliable information about P_{y+} comes from linear dichroism and hole-burning results.[15−17] Low-temperature linear dichroism measurements of *Rp. viridis* by Breton et al.[15] revealed two excitonic absorption bands assigned to the special pair; the lower energy band (P_{y-}) absorbed at 990 nm, while the upper band was observed at 850 nm exhibiting a negative linear dichroism and was assigned as P_{y+}. The P → P_{y+} transition carried one-tenth the oscillator strength of P → P_{y-}, and its transition dipole

* To whom correspondence should be addressed.
† Department of Education GAANN Predoctoral Fellow.
‡ Department of Chemistry, Unversity of Pennsylvania.
§Department of Biochemistry and Biophysics and Johnson Foundation, University of Pennsylvania.
|| Alfred P. Sloan Foundation Fellow.
⊥ University of Chicago.

10.1021/jp984464j CCC: $18.00
Published on Web 03/04/1999

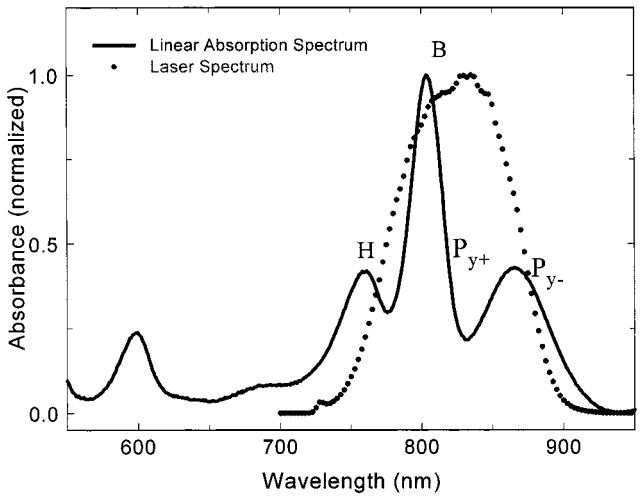

Figure 1. Near-IR absorption spectra for the photosynthetic reaction center of *Rhodobacter sphaeroides*. The three major bands are labeled as resulting from absorptions due to the bacteriopheophytins at 760 nm (H), accessory bacteriochlorophylls at 800 nm (B), and the special pair (P_{y+} and P_{y-}) at 825 and 870, respectively. The dotted line represents a sample laser spectrum. The center wavelength of the spectra is tunable from 750 to 850 nm.

moment was rotated by 60 degrees with respect to the P → P_{y-} transition moment. Linear dichroism measurements for *Rb. sphaeroides* gave similar results, with P → P_{y-} at 890 and P → P_{y+} at 810 nm. The results obtained by Breton[15] were supported by hole-burning studies from Small and co-workers.[16,17] Upon burning a hole in the P_{y-} absorption band, distinct bleach bands were observed at 848 nm (*viridis*) and 811 nm (*sphaeroides*) due to depletion of the P → P_{y+} transition for each species. The polarization characteristics suggested that the P_{y+} bands were nearly orthogonal to the P_{y-} band and the intensity ratios were approximately 10 to 1.

The hole-burning and linear dichroism results provide fairly convincing proof that P_{y+} absorbs near 810 nm for *Rb. sphaeroides* at 15 K. However, neither the transition energy nor the oscillator strength has been determined for P_{y+} at room temperature. Such information would provide valuable insight into the electronic character of the special pair. The principal reason for the lack of room-temperature information is the spectral congestion in the (anticipated) region of P → P_{y+} absorption due to overlap with the strong B and P_{y-} absorption bands, making it very difficult to deconvolute individual spectra.

Energy transfer from the accessory bacteriochlorophyll to the special pair has been observed experimentally by various pump−probe techniques that detect a bleaching of the P_{y-} band due to energy transfer from B,[18] emission from the excited state of P_{y-},[19] or transient absorption from P_{y-}.[20] Breton and co-workers[18] observed identical rise times in the bleach of the P_{y-} band after excitation of P, B, or H with 100 fs pulses, suggesting that energy transfer from B to P must occur on a 100 fs or shorter time scale. Haran et al.[19] have reported rise times of 118 fs for stimulated emission of P_{y-} upon excitation of B and P_{y+} at 810 nm in *Rb. sphaeroides*. Haran et al.[19] used a series of anisotropy measurements with excitation at 810 nm and detection at longer wavelengths (950, 1215, and 3840 nm) to investigate energy transfer. The observed kinetics combined with observed anisotropy values suggested that energy transfer should be thought of as an internal conversion process between adiabatic supermolecular states. Specifically, the energy transfer between B and P_{y-} is proposed to occur from a B/P_{y+} mixed state to a state of mostly P_{y-} character.

More recently, Jonas et al.[20] have reported pump−probe anisotropy measurements of the R-26 strain of *Rb. sphaeroides* with 25 fs pulses centered at 799 and 805 nm. The resulting temporal traces containing signals due to B, P_{y+}, and P_{y-} were analyzed using published crystallographic orientations and assumed transition moment directions and spectra for each species. A kinetic scheme for energy transfer of B → P_{y+} → P_{y-} with time constants of 80 and 150 fs yielded the best fit to their data. The rapid energy-transfer dynamics were inconsistent with rates derived using Förster (weak coupling) theory,[21] which predicts rates for B → P_{y+} → P_y energy transfer that are at least an order of magnitude slower than the observed rates.[22] The inadequacy of weak coupling Förster theory led Jonas et al. to suggest a strong coupling or coherent mechanism for energy transfer.

The Boxer group reported the results of experiments that measured the spontaneous emission from P_{y-} after excitation at various wavelengths throughout the 800 nm band and as a function of temperature.[23] These experiments showed two important results. First, excitation into the assumed P_{y+} band with pulses at 825 nm led to a more rapid rise in the emission from P_{y-} than did excitation at 800 nm. The rapid excitation of P_{y-} following optical excitation into P_{y+} is consistent with the model put forth by Jonas et al.,[20] but the time scale for internal conversion between the excited states of P is not. Second, the temperature dependence of the energy-transfer rates was small despite the large change in spectral overlap between B and P. The authors contended that this precludes Förster mechanisms, which depend on the spectral overlap, from playing a major role in the energy/excitation transfer process. [23]

This paper presents the results of "two-color" wavelength-resolved pump−probe anisotropy measurements. The major Q_y absorption bands are collectively excited using a short (13−18 fs) pulse with a broad spectral range or individually excited with longer pulses that are spectrally narrowed to overlap with the transition(s) of interest. A spectrally broad-band probe is then used to detect the response of the entire system with respect to wavelength, time, and polarization. Results are presented for collective excitation, as well as selective excitation of P_{y-}, P_{y+}, B, and H. The extent of the interchromophore coupling is explored via time-resolved experimental methods with respect to two physical observables: the excitonic splitting of the special pair and energy-transfer rates between individual cofactors or excitonic states. Optical excitation of the lower excitonic state, P_{y-}, at 870 nm yields information about the excitonic splitting of the special pair and provides the first room-temperature characterization of P_{y+}. The dynamics associated with the P_{y+} state are investigated further by direct excitation at the P_{y+} absorption peak, determined here to occur at 825 nm. These results indicate that internal conversion of P is rapid, occurring with a 65 fs time constant. Spectrally overlapping transitions that prevented previous determination of the energetics and dynamics associated with P_{y+} are dealt with through the precise measurement of relevant chromophore spectra obtained as a function of wavelength and time after excitation at various points across the Q_y absorption bands. These measurements are performed using parallel, perpendicular, and magic-angle pump−probe pulse pairs. It has been possible to separate the various spectra contributing to the transient transmission signals by virtue of their time dependence and anisotropy. Finally, excitation at 800 nm allows for the investigation of energy transfer from B to P_{y-}. The wavelength-resolved results indicate that energy transfer from the excited accessory bacteriochlorophyll, B*, to the lower excitonic state of the special pair, P_{y-}, occurs

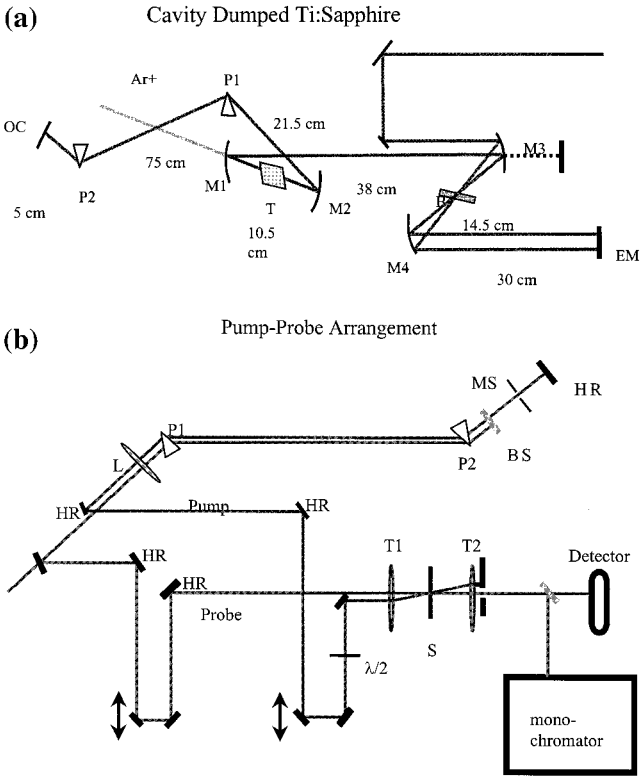

Figure 2. Experimental apparatus. A schematic of the cavity-dumped Ti:sapphire oscillator is shown in panel a, while panel b illustrates the pump−probe apparatus used (a) Oscillator: M1−M2, 10 cm radius of curvature (ROC) mirrors (CVI TLM2); M3−M4, 15 cm ROC mirrors (CVI TLM2); OC, 97.8% output coupler (CVI PR2); T, Ti:sapphire (Crystal Systems, 3.5 mm); EM, high reflector (CVI TLM2); B, Bragg cell (Harris H-101). M3 extension: end mirror for "four-mirror cavity" before cavity-dumping adaptation. (b) Pump−probe arrangement: P1−P2, fused silica prisms; BS, beam splitter; MS, mechanical slit; HR, high reflector; NM1−NM2, Nanomover (Melles Griot) variable delay lines; $\lambda/2$, half wave plate; T1−T2, Cassegrain telescopes; S, spinning cell sample holder.

by a two-step mechanism, with the upper excitonic state (P_{y+}) serving as the kinetic intermediate. Excitation relaxation in reaction center samples that contain oxidized special pairs will be discussed, and an alternative pathway for relaxation will be suggested.[24−26] Coherence in the excitation transfer from B* to P_{y+} and the contrast with linear and nonlinear responses of the oxidized sample strongly suggest a supermolecular description of the states B, P_{y+}, and P_{y-} at early times after excitation.

The results of this paper monitor the energy/population dynamics of several of the Q_y band excitations and electronic states of this reaction center. This information is complementary to that obtained from optical dephasing studies characterizing the time scales and magnitudes associated with electronic energy gap fluctuations of the same reaction center energy levels. The results of the coherence studies are another publication in a series.[27] A preliminary account of the present paper were given elsewhere.[76]

II. Experimental Section

A. Pump−Probe Spectrometer. The experiments reported here were all performed with the optical pulses generated by a home-built cavity-dumped Kerr lens mode-locked Ti:Sapphire laser.[28,29] The design of the laser is illustrated in Figure 2a, while the pump−probe experimental setup is shown schematically in Figure 2b. The laser produces optical pulses with (Gaussian) spectral bandwidths of 60−100 nm fwhm, temporal durations of 12−15 fs, and little chirp, as verified by TG-FROG-type

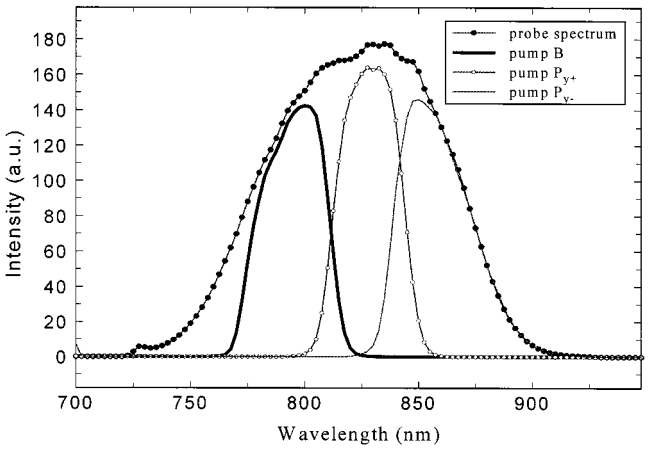

Figure 3. Wavelength-resolved pump−probe spectra. The excitation and probe spectra used for obtaining wavelength-resolved pump−probe measurements are shown. The gray line indicates the spectrum for the broad-band probe, while the other lines represent pump spectra designed to overlap P_{y-}, P_{y+}, and B, respectively.

measurements.[30,31] A typical laser spectrum centered at 830 nm is shown in Figure 1 superimposed on the absorption spectrum of the reaction center. The center wavelength of the cavity-dumped laser output is tunable throughout the near-IR absorption bands of the reaction center, with spectral peak values ranging from 760 to 850 nm by the selection of an appropriate mirror set for the cavity. A decrease in spectral bandwidth is observed when the laser spectrum is centered near either extreme of this range.

The pump−probe experimental scheme (Figure 2b) is different from those previously used by this group.[28,32] In previous experiments, the output of the laser made forward and return passes through a pair of fused silica prisms to compensate for positive group velocity dispersion (GVD) prior to being split into pump and probe beams with variable time delays. In the present experiment, however, the output of the laser is split into pump and probe beams after the forward pass through the prism-pair compensation line. This is accomplished with a thin window placed between the second prism and the high reflector (HR) at the end of the compensation arm (see Figure 2). The back surface reflection from the beam-splitting window (10%) retraces the prism path vertically displaced (above) the incoming beam and serves as the broad-band probe. The remaining 90% portion of the beam not reflected by the beam-splitting window passes through a pair of razor blades (mechanical slit) that allows spectral selection of the pump beam.[33] The HR then reflects the spectrally narrowed beam back vertically displaced below the incoming beam. This method of spectral selection allows for complete control of the pump spectrum within the broad envelope of the probe and provides many advantages over other methods of spectral selection (i.e., interference filters) in that the amount of material in each arm is equal. Furthermore, the pump spectrum may be changed without inducing any temporal shift in the zero of time. Representative pump spectra used in the measurements presented below are shown in Figure 3 superimposed on the reaction center spectrum. These laser pulse spectra were chosen to give maximum overlap with the B, P_{y+}, and P_{y-} bands, respectively. Figure 3 also indicates the broad probe spectrum, capable of detecting changes in the absorption characteristics of multiple bands after selective excitation with any given pump pulse.

Following dispersion compensation and pump spectral selection, the pump and probe beams are sent through two variable delay lines and focused into the sample with a Cassagrain telescope ($f_1 = 20$ cm, $f_2 = -50$ cm) to a spot size of less than

200 μm in diameter. The zero of time and instrument response function are determined by the cross-correlation of the two beams in a 100 μm thick KDP crystal and also via in situ solvent scattering responses. For wavelength-resolved pump−probe measurements, the transmitted probe beam is dispersed by a 0.25 m monochromator (CVI Laser) selecting a 3 nm bandpass and detected using an avalanche photodiode (Hamamatsu). The pump-induced modulation is processed with a lock-in amplifier (Stanford SRS-830) referenced to the chopping frequency.

B. Data Analysis and Processing. The primary experimental technique utilized in this work, wavelength-resolved anisotropy, is obtained by monitoring the spectrally resolved probe transmission as a function of temporal delay and polarization relative to the pump. The time- and wavelength-resolved anisotropy is calculated from the pump−probe signals as

$$r(\lambda,t) = \frac{S_{\mathrm{par}}(\lambda,t) - S_{\mathrm{per}}(\lambda,t)}{S_{\mathrm{par}}(\lambda,t) + 2S_{per}(\lambda,t)} \tag{1}$$

where $S_{\mathrm{par}}(\lambda,t)$ and $S_{\mathrm{per}}(\lambda,t)$ are time and wavelength-resolved pump−probe transients obtained with parallel and perpendicular pump and probe polarizations, respectively. Wavelength-resolved anisotropy measurements were used to distinguish spectral components based on both the spectral properties and transition moment spatial orientation. The anisotropy associated with optical detection of a particular transition depends on the angle (θ_{ij}) between the prepared (pumped) and detected (probed) transitions through the following relation.

$$r(\theta_{ij}) = \frac{1}{5}[3\cos^2(\theta_{ij}) - 1] \tag{2}$$

The sensitivity of induced probe transmission to the orientation of the probed transition can be removed if the experiments are performed with the polarization difference between the pump and probe pulses set at 54.7°, the magic angle. The magic-angle signal then depends only on the pump-induced population change of each state, independent of the orientation.

Experimentally, the parallel and perpendicular pump−probe signals are obtained in alternating fashion to minimize the effects of slow drift in alignment, laser power, or sample quality. Typically, a few temporal delay or detection wavelength scans performed with parallel pump and probe pulse pairs are followed by similar data sets obtained under perpendicular polarization conditions. This process is continued until 10−12 scans have been performed with both polarization conditions.

Two methods of data analysis and fitting are used to process temporally or spectrally resolved data. Temporally resolved data sets (i.e., a pump−probe signal with a constant detection wavelength) are analyzed using a linear prediction singular value decomposition (LPSVD) routine that fits the data to a series of exponentially damped cosine functions with either zero (pure exponential decay) or finite (oscillatory) frequencies.[32]

$$\mathrm{SVD}(t) = \sum_i a_i e(-t/\tau_i)\cos(\omega_i t + \varphi_i) \tag{3}$$

where a_i, τ_i, ω_i, and φ_i represent the amplitude, decay constant, frequency, and phase of the ith oscillatory term, respectively. In this representation, the exponential decay terms are indicative of population dynamics while the oscillatory terms reveal the frequencies and dephasing rates of vibrational or electronic coherences established in the system. In almost all cases, the frequencies returned by the SVD algorithm reproduce those obtained by Fourier analysis of the signals. When relevant, the Fourier power spectrum of the time-domain signal is included with the result.

All simultaneous time- and wavelength-resolved pump-induced probe transmission spectra reported herein are considered to be comprised of a series of Gaussian components $S(\lambda,t)$.

$$S(\lambda,t) = \sum_i \left\{ a_i(t)\, e^{-\left(\frac{\lambda - \lambda_{0i}}{w_i}\right)^2} \right\} \tag{4}$$

where $a_i(t)$, λ_{0i}, and w_i are the amplitude, peak wavelength, and width of each component contributing to the spectra at a given pump−probe delay time, t. Note that the widths reported here are not full widths at half-maximum. Convoluting the fitted Gaussian line shape components with the finite pulse spectrum reproduces the experimentally obtained spectra. Two comments are worthwhile concerning the presentation of experimental data in this paper. First, the data as presented are not normalized for the finite pulse spectrum (60−100 nm fwhm). Second, the data are presented as a change in transmission; transient gain results in a positive signal, while absorption yields negative magnitude (spectral) components.

C. Sample. The reaction center samples were isolated from the carotenoidless R-26 strain of the purple bacteria *Rhodobacter sphaeroides* according to the published procedure by Clayton and Wang[34] and further purified by FPLC. The isolated reaction centers were suspended in a Tris buffer (pH 8) with the detergent LDAO (lauryldimethylamine oxide), DTT (dithiothreitol), and HNQ (2-hydroxy-1,4-naphthoquinone); the latter two serve to reduce the quinone, Q_A. The room-temperature samples are contained in a 0.5 mm path length airtight spinning cell rotating at 20 Hz. Typically, the samples are interrogated at a radius of 9 mm from the axis of rotation. The resulting sample linear velocity of 11.3 m/s is sufficient to ensure that each laser pulse interacts with a fresh sample, given a 2 kHz pump (4 kHz probe) repetition rate and a 175 μm spot size.

For all the experiments presented here, the pulse energies entering the sample were 10 nJ for full pump excitation (no spectral selection) and 1 nJ for the probing pulse. The Cassegrain telescope ($f_1 = 20$ cm, $f_2 = -50$ cm) focuses the beam to a spot of approximately 175 μm diameter as judged by pinholes and verified by Gaussian beam analysis.[35] These focusing conditions give a photon density in the sample of 1.33×10^6 photons/μm^2, allowing each pulse to excite approximately 5% of the 2×10^{-5} M reaction centers. Generally, the transient transmission signals, $\Delta T(t)$, shown in the figures below were only a few percent modulation on the nominal probe beam intensity.

There are three potential sources of signal distortion that must be considered when using this type of sample arrangement. The first arises from the possibility that successive laser pulse pairs will interact with the same sample. With the excitation conditions used in these studies, however, the excited sample area moves more than 0.5 mm during the time between pump−probe pulse pairs, guaranteeing a fresh sample for each laser shot. Second, there is also the possibility of interrogating reaction centers that have not recovered from the charge-separated state ($P^+Q_A^-$), which decays to the initial ground state with a 100 ms time constant. However, for the excitation conditions used, each reaction center will have an opportunity (in the sense of spatial overlap) to interact with the laser excitation beam once every three revolutions on average, yielding an average recovery time of 150 ms. This, combined with the fact that only a small percentage of the reaction centers in the excitation

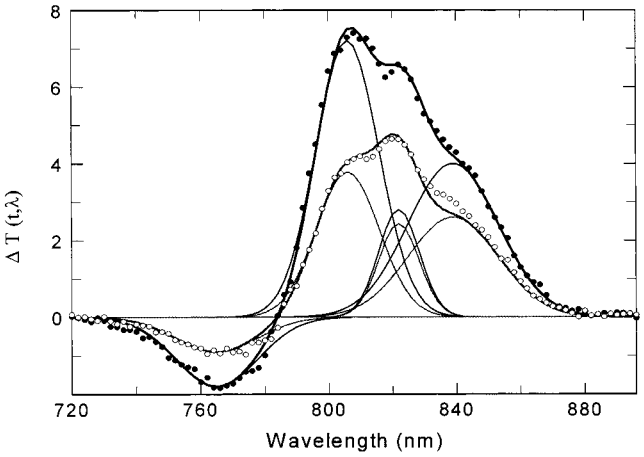

Figure 4. Pump−probe anisotropy spectra obtained (200 fs) after excitation at 800 nm with a broad-band pulse: parallel pump−probe data, filled circles; perpendicular pump−probe data, open circles. The four components typically observed in the wavelength-resolved pump−probe experiments of the RC are highlighted as Gaussian line shapes for parallel and perpendicular polarizations. See text for details.

volume are pumped to an electronically excited state by a given laser pulse, ensures that the number of charge-separated RCs that are optically reinterrogated is minimal.

The third, and potentially most important, source of signal degradation results from reaction centers absorbing two photons from the same laser pulse. Jonas et al. investigated this saturation condition in some depth.[20] They found that saturation due to doubly excited RCs was a significant problem and resulted in both a decreased quantum yield of electron transfer and distorted kinetics. The experimental conditions in that instance were such that the photon density was 1.4×10^6 photons/μm^2. At that energy density, 7% of the reaction centers absorbed a photon and the quantum yield for charge separation was reduced by 6% from the ideal value. If the energy density of the pump beam utilized in those studies was increased, the pump−probe signal exhibited saturation effects and a 300 fs decay component appeared in the relaxation of B* excitation.

III. Results

A. Broad-Band Excitation. The wavelength- and polarization-dependent transient probe transmission recorded for a delay time of 200 fs after broad-band excitation at 800 nm is shown in Figure 4. Under these excitation conditions, all of the Q_y optical bands of the reaction center, particularly those pertaining to the accessory bacteriochlorophylls and the special pair are (perhaps coherently) excited and should contribute unique anisotropy and spectral characteristics to the total signal. The transient transmission spectra shown in Figure 4 display four features commonly observed in all of the wavelength-resolved anisotropy measurements: strong bleach/stimulated emission signals at 800, 825, and 870 nm as well as a transient absorption, seen here as a negative signal at 770 nm. The spectral position (after convolution with the laser spectrum) and polarization ratio of each of the four components is highlighted on the plot by showing the individual spectral components for parallel (larger magnitude Gaussian) and perpendicular (smaller magnitude) pulse pairs. The center wavelengths listed are for Gaussian spectral widths convoluted with the laser spectrum to yield a fit to the experimental results. The transient transmission spectral data has *not* been normalized to account for the finite pulse spectrum. Rather, the pulse spectrum is accounted for in the fitting process via frequency domain convolution.

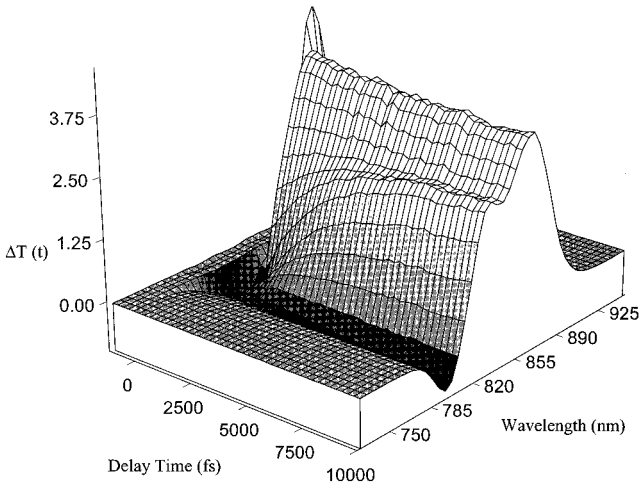

Figure 5. Pump−probe transient transmission signals following excitation of P_{y-} with an optical pulse centered at 860 nm. The three-dimensional surface represents the pump-induced transient transmission of the broad-band probe for time delays of 0−10 ps. Data shown is for parallel pump and probe polarizations. The transient contains spectral waveforms characteristic of stimulated emission from P_{y-}, ground-state bleach of P (both P_{y-} and P_{y+} transitions), excited-state absorption from P_{y-}, and electrochromic shift of the accessory bacteriochlorophyll.

It is seen that the most prominent spectral component for short delay times, such as that shown in Figure 4, is a strong bleach at 800 nm arising from B* excitation and depletion of ground-state B.[36,20] Under mild excitation conditions, this feature decays rapidly, with a time constant of less than 100 fs.[20] At higher excitation fluence, as discussed below in Figure 18, the decay exhibits a significantly slower component ($\tau = 300$ fs).[37] In addition to the bleach associated with B at 800 nm, there is also a noticeable feature at 825 nm with an anisotropy greatly reduced from that of either the 800 nm band or the 870 nm band. The origin of this band is one of the major questions addressed in this paper. It will be shown later that this transition is bleached upon excitation of P_{y-} with an optical pulse centered at 860 nm and yields polarization characteristics consistent with those expected for the upper excitonic state, P_{y+}.[15] The energetic position of this band, halfway between B and P_{y-}, suggests that it may play a role in energy transfer from B to P_{y-}. Finally, the long wavelength bleach/gain band at 840 nm and beyond in this figure corresponds to the blue edge of the $P \rightarrow P_{y-}$ transition observed in Figure 1. The finite laser bandwidth precludes observation of the entire band.

B. Excitation at 860 nm: Observation of P_{y-}. The full response of the photosynthetic reaction center to optical excitation of the special pair at 860 nm as a function of time and wavelength for parallel pump and probe pulse polarization is shown in Figure 5. Exclusive excitation of the special pair is obtained by mechanically limiting the pump spectrum as described in the Experimental Section. Figure 6 shows the parallel and perpendicular polarization pump−probe signals obtained under identical excitation conditions as for Figure 5 but for a delay time of 100 fs; that is an early delay time spectral slice through the data. In both cases (Figures 5 and 6), the transients show complex responses consisting of photo bleaching (gain) at 860 and 825 nm, a transient absorption near 800 nm, and a derivative-like component (minimum at 790 nm, maximum at 814 nm) that becomes dominant at longer delay times. The complex nature of the responses seen in Figures 5 and 6 illustrates the necessity of characterizing each component by its spectrum, anisotropy, and temporal dependence if information about their identity is to be garnered.

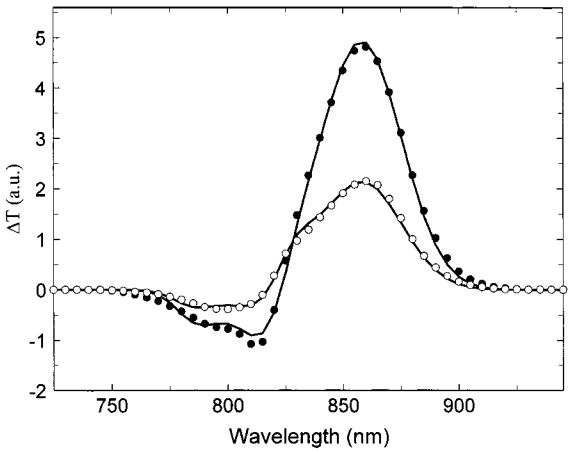

Figure 6. Wavelength-resolved anisotropy measurements obtained 100 fs after excitation of the special pair at 860 nm: parallel pump−probe data, filled circles; perpendicular pump−probe data, open circles. The solid lines through the data represents a fit to the data using spectral components corresponding to P_{y-}, P_{y+}, P^+H^-, and P_{y-} (absorption). The spectra, anisotropies, magnitudes, and temporal characteristics of each component are summarized in Table 1.

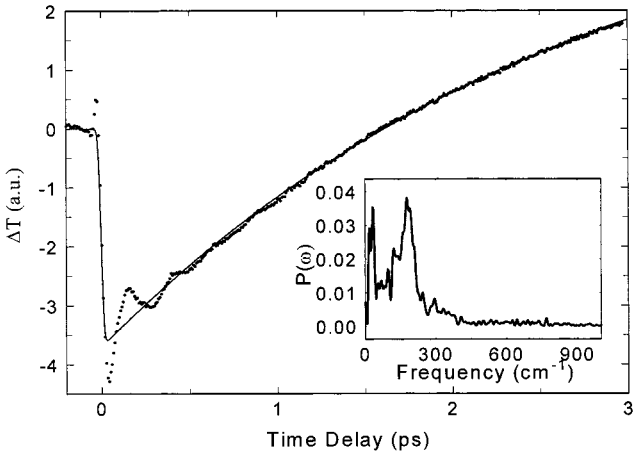

Figure 7. Transient absorption dynamics from P_{y-}. The pump−probe signal is shown for excitation at 860 nm, with detection at 800 nm. A negative signal indicates transient absorption, while a positive signal indicates a photobleach: circles, experimental data; solid line, bi-exponential fit incorporating one decaying exponential (absorption) and one rising exponential corresponding to a buildup of bleach. Both exponential components have a time constant of 2.8 ps. The inset shows the deconvoluted Fourier power spectrum of the residual following exponential fitting of the temporal data.

The positive band around 860 nm matches (after allowing for the finite extent of laser spectrum) the spectrum for the P $\rightarrow$ P_{y-} transition and is therefore identified as stimulated emission from P* and/or bleach due to depletion of the P ground state. Under these excitation conditions, the 870 nm feature exhibits a strong anisotropy $r(100\ \text{fs}) = 0.33$ that decays on 50 fs and tens of picoseconds time scales. The slow decay is indicative of ground-state bleach recovery of the special pair after optical excitation. This identification of the origin of the slow component is supported by the absence of a 3 ps decay, which would indicate the decay of P* due to electron transfer. The rapid (i.e., 50 fs) decay observed here (as will be discussed more later) results from a very fast Stokes shift of P_{y-}.[38]

In addition to the 870 nm feature in Figure 6, a bleach is observed near 825 nm, appearing as a distinct shoulder on the low-wavelength side of the broad bleach near 870. This component is more prominent in the perpendicular trace than in the parallel, suggesting a negative anisotropy. Such an anisotropy value corresponds to a transition dipole moment rotated to an angle greater than 54.7° from the P $\rightarrow$ P_{y-} transition. The exact angle depends sensitively on the anisotropy for this band, which in turn, depends on the relative amplitude of this band and others contributing at 825 nm, such as the broad transient absorption near 800 nm. The lines through the data points in Figure 6 represent a spectral/temporal fit described below.

The structured absorptive feature near 800 nm is similar to that observed by Vos et al.[38] They assigned the transition to excited-state absorption from P_{y-}. The structure of this absorptive feature was thought to arise from changes in the excitonic interactions between all six reaction center pigments upon formation of the P_{y-} excited state. The present measurements support the assignment of the overall absorptive feature to excited-state absorption from P_{y-}. It is possible that the structure observed in these spectra corresponds to shifts in the 800 nm bands after excitation of the special pair. Two comments are in order with respect to this issue. First, the anisotropy of the entire absorptive feature is identical to that observed for the bleaching of the P $\rightarrow$ P_{y-} transition at 870 nm. Second, temporal pump-probe experiments interrogating this spectral region after excitation at 860 nm reveal that oscillatory components consistent with the special pair marker mode are observed across the entire absorptive band. The time dependence of the absorptive feature, as well as the growth of a bleach component due to selective detection of the derivative-like shape, is shown in Figure 7. Here, the broad-band probe is detected at 800 nm after excitation at 860 nm. This is equivalent to taking a slice of Figure 5 along $\lambda = 800$ nm. Two components are necessary to fit the data, a negative decaying exponential and a positive growing exponential. The time constant for both features, $\tau =$ 2.8 ps, is the same as the charge-transfer time.[39,40] The exponential terms are convoluted with the instrument response; no finite rise or induction time is necessary to adequately fit the data (see Figure 7). Fourier and SVD analyses indicate that the oscillation observed in the decay corresponds to a vibrational mode with a frequency of 140 cm^{-1}(see inset to Figure 7), in good agreement with the oscillations observed by Vos et al. and[41−43] Stanley et al.[44] for the marker mode of P_{y-}. We treat the absorptive feature, including the fine structure, as one spectral component associated with P_{y-} excited-state absorption. This is validated by the anisotropy in this region and the strong presence of the special pair marker mode.

The final feature present in the data sets of Figures 5 and 6 is a derivative-like shape exhibiting an absorption maximum at 790 and a bleach maximum at 814 nm. As indicated in Figure 7, this feature appears with the charge-transfer time, exhibiting a 2.8 ps rise. This shape is generally considered to arise from an electrochromic shift of the accessory bacteriochlorophyll (B) after generation of the charge-separated state, P^+H^-.[45] The spectrum observed at long temporal delays (10 ps) indicates that the induced electric field amounts to a 12 nm blue shift in the spectrum of B, in good agreement with previous results.

The wavelength-dependent parallel and perpendicular pump−probe data are fit with a series of spectra corresponding to P_{y-} (ground-state bleach/stimulated emission), P_{y+} (ground-state bleach), P_{y-} (excited-state absorption), and P^+H^- (electrochromic shift of the B transition due to presence of a charge-separated state), each with it's own anisotropy and temporal dependence. A sequence of spectra and anisotropy curves similar to those presented in Figure 6 are fit self-consistently for time delays of 0−1 ps. The resulting ground-state spectra for P_{y+} and P_{y-} were also used to simulate the steady-state absorption

TABLE 1. Anisotropy Analysis of Special Pair Features[a]

component	wavelength (nm)	width (nm)	amplitude[b]	anisotropy pump at P_{y-}	exponential time dependence
P_{y-}	870	34	1	0.33 (±0.02)	50 fs decay >20 ps decay
P_{y+}	825	16	0.18 (±0.04)	−0.05 (±0.03)	>20 ps decay
P_{y-}[b] (absorption)	816/795	16/24	0.38 (±0.08)	0.33 (±0.02)	2.8 ps (±0.3) decay
P^+H^-	810/790	14	0.3 (±0.05)	∼0	2.8 ps (±0.3) rise

[a] This table shows a summary of the spectral components used for fit the time and wavelength pump probe and anisotropy transients after excitation of the P → P_{y-} band with an optical pulse centered at 860 nm. All the amplitudes listed here are peak absorption coefficients, normalized to that of the P_{y-} bleach. Likewise, anisotropy values are relative to the excited P → P_{y-} transition. Widths are listed according to the definition in eq 4. [b] Amplitudes normalized to the P_{y-} bleach signal.

spectra, in addition to (Gaussian) bands near 800 nm (B) and 760 nm (H). The energy, width, magnitude, anisotropy, and temporal behavior for each spectral component that contributes to the best fit for the pump−probe absorption spectra and the steady-state absorption spectra are given in Table 1. The reported amplitudes are all relative to the P_{y-} component, which has been normalized to 1. The results of the fitting procedure for a delay 100 fs delay after excitation at 860 nm are shown as the lines through the data points in Figure 6.

As indicated in Table 1, the optical transition to the upper excitonic state (P → P_{y+}) is found to have an energy corresponding to absorption at 825 nm and has an anisotropy of −0.05 (±0.03) with respect to the P → P_{y-} transition. In comparison with the P → P_{y-} band, the P → P_{y+} band is significantly narrower, by about a factor of 2, and has a peak extinction coefficient that is 18% of that for P_{y-}. Hence, the ratio of integrated transition strengths for P_{y+}/P_{y-} is close to 1:10. This measured dipole moment direction and transition strength are in reasonably good agreement with results from low-temperature studies by Breton.[15] However, the transition energy is not in agreement with the low-temperature results that placed P_{y+} at 810 nm. The room-temperature value of 825 nm implies that either the special pair intradimer excitonic coupling or the P_L and P_M monomeric transition energies decreases with an increase in temperature. A temperature-dependent analysis of this splitting may provide useful information about the conformational and energetic changes induced by lowering the temperature.

C. Time Domain Anisotropy Probes of Exciton Interactions. The excitonic interactions of the special pair have been measured through time domain anisotropy techniques. A series of papers from the Hochstrasser group[46,47] indicate that unique anisotropic decays are to be expected if degenerate or nearly degenerate transitions are coherently excited with a short laser pulse. For the particular case of a dimer, the anisotropy is predicted to oscillate with a frequency that corresponds to the energetic splitting between the two excitonic levels. The decay of the oscillation reflects loss of the phase relationship between the two excitonic levels and the rate of population equilibration between the two levels. Nonclassical initial anisotropy amplitudes[48] and coherent oscillations[49,50] have recently been observed in a number of native and isolated light-harvesting systems.

The time domain pump−probe signals obtained with parallel and perpendicular pulse pairs are shown in Figure 8a. For this measurement, the pulses have a 80 nm fwhm bandwidth centered at 850, sufficient to excite a coherent superposition of the P_{y+} transition at ∼825 nm and the P_{y-} transition at 865 nm. The data shown correspond to wavelength-integrated detection. The anisotropy calculated from the pump−probe signals is displayed as points in Figure 8b. The decay of the initial anisotropy from the classical limit of 0.4 to a final level of 0.32 occurs with an exponential time constant of 60 fs. The general decay of the anisotropy can be fit by two exponential components with time

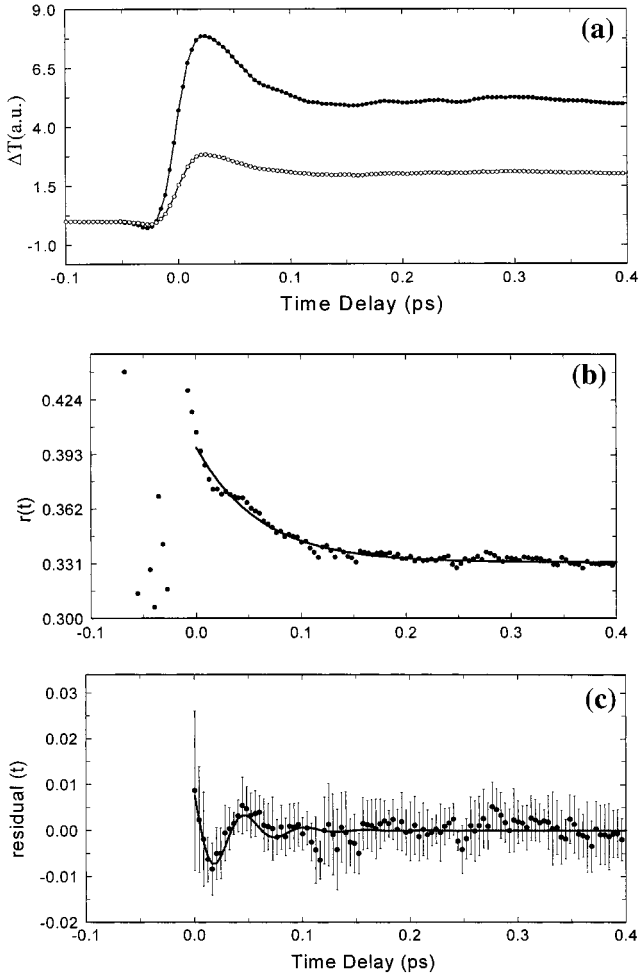

Figure 8. Time domain anisotropy of special pair obtained after excitation of the special pair with a broad-band optical pulse centered at 850 nm (80 nm fwhm). The full wavelength-integrated response is reported. (a) Pump−probe signals obtained with parallel (solid circles) and perpendicular (open circles) polarizations. (b) The anisotropy calculated from the pump−probe data in panel a according to eq 1; Experimental anisotropy data, solid points. The line through the data is a biexponential fit. See text for details. (c) Oscillatory behavior of anisotropy. The solid points indicate the residual anisotropy after subtraction of the exponential fit (panel b). The solid line indicates a fit to the data with a damped cosine curve. The least-squares fitting procedure returns a frequency of 593 cm^{-1} and a damping constant of 35 fs for the oscillatory feature. The exponential decay was characterized by two exponential components with decays of $\tau_1 = 59$ fs and $\tau_2 = \infty$ and amplitudes of 0.065 and 0.33, respectively.

constants of 60 fs and >20 ps (the latter is not well defined with these data). The solid line through the anisotropy data points represents this exponential fit. The 60 fs decay in the anisotropy results (as discussed below) from rapid thermalization or equilibration of the two excitonic energy levels P_{y+} and P_{y-}.

The residual obtained by subtracting the biexponential fit to

the anisotropy of Figure 8b is shown in Figure 8c. (The error bars represent the standard deviation of anisotropy points calculated from individual pairs of parallel and perpendicular pump−probe transients.) Visual inspection reveals that the residual deviates significantly from zero at early times, indicating that the anisotropy decay is not simply exponential but has a considerable oscillatory component. The line through the residual represents an exponentially damped cosine function, with the best-fit value for the frequency of 593 cm^{-1} (±20) and a damping time of 35 fs. The formalism for exciton dynamics in anisotropy measurements developed by Hochstrasser et al. indicates that this oscillation frequency is a direct measure of the excitonic splitting for the dimer. Accordingly, the upper excitonic transition should absorb at 823 nm, 593 cm^{-1} higher in energy than the 865 nm P → P_{y-} transition. This placement of P_{y+} is in good agreement with the assignment in the previous subsection based on the spectrally resolved anisotropy data. If the P_{y+} energetics were such that the P → P_{y+} transition was at 810 nm, as is frequently assumed based on low-temperature hole-burning experiments, the oscillatory frequency observed via anisotropy experiments would be approximately 785 cm^{-1}, nearly 200 cm^{-1} above the observed frequency.

Analogous dimer splitting information has recently been obtained through anisotropy techniques for the B820 dimer of bacteriochlorophyll *b* molecules extracted from *Rb. rubrum* LH1 aggregates.[50] The excitonic splitting observed for B820 dimers is significantly smaller than that observed here for the reaction center, underscoring the strongly coupled nature of the special pair. Considerable information about the monomer−monomer coupling site inhomogeneities can be obtained from more extensive experiments and analysis than that presented here.

D. P_{y-} Stokes Shift Dynamics. Previous experiments by the Martin[41−43] and Boxer[44] groups have indicated that the Stokes shift dynamics for P* are fast. Using 50−80 fs pulses, Stanley et al.[44] observed an instrument response limited rise in the fluorescence from P_{y-} at 940 nm. Here, we investigate the rapid Stokes shift of P_{y-} by exciting the special pair with a broad-band pulse centered at 850 nm and detecting either the wavelength-integrated signal or the wavelength-resolved transient at 930 nm with a parallel polarized degenerate probe. The pump and probe pulse spectra are strongly overlapped with the P → P_{y-} absorption but not with the P_{y-} → P emission spectrum centered at 930 nm. Hence, detection of the entire probe beam will be sensitive mostly to the ground-state bleach of P, although stimulated emission from a "nonrelaxed" excited state may contribute to the signal at early times. If only the extreme red edge of the probe beam is detected then stimulated emission from P_{y-} will dominate the signal, provided that the detected portion of the stimulated emission is well separated from the absorption at 865 nm. It is possible, however, that the 50 fs component results from stimulated emission prior to P_{y-} moving out of the range of detection, i.e., Stokes shifting.

Figure 9a shows the pump−probe signal for wavelength-integrated detection following broad-band excitation of P_{y-}. The time-dependent transient shows a rapid decay followed by a slowly decaying ground-state bleach. The data are well fit with a biexponential decay convoluted with the instrument response function (∼15 fs pulse). The best fit is obtained with time constants of 50 fs and 20 ps, the latter of which is not well determined with this data time window. A 2.8 ps component corresponding to the time scale for charge-transfer[39,40] is not observed, suggesting that the slow decay is entirely due to ground state bleach relaxation and/or recovery. The deconvoluted Fourier power spectrum shown in the inset indicates that low-frequency modes (140 cm^{-1}) are dominantly coupled to the optical transition.

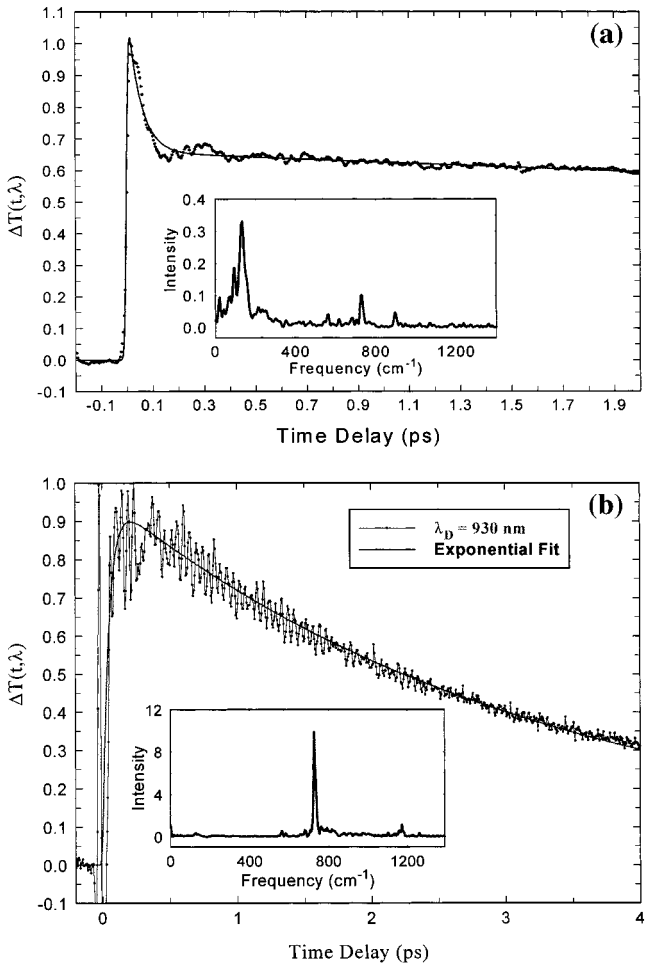

Figure 9. Transient pump−probe measurement of Stokes shift dynamics in P_{y-} after excitation at 850 nm. (a) Pump−probe signal obtained for wavelength-integrated detection. The line through the data shows a biexponential fit with components of 50 fs and ∼20 ps. (b) Pump−probe signal detected in the region of stimulated emission at 930 nm. The experimental data points are shown connected by the line, while the dark black line through the data is a fit with a 2.8 ps decay following a 50 fs rise time. The insets in parts a and b of Figure 9 are the Fourier power spectra of the oscillatory residuals.

In contrast to the wavelength-integrated data, the signal obtained for detection at 930 nm, displayed in Figure 9b, shows a delayed rise (following with the derivative-like cross-phase modulation at $T = 0$) for 930 nm detection and an approximately 3 ps decay signifying sensitivity to the charge-transfer process and depletion of P_{y-} population. In particular, the solid line through the data consists of two components; a rising exponential of 50 fs preceeding a 2.8 ps decay is necessary to fit the transient waveform. The 50 fs decay near 870 nm and a corresponding rise in the stimulated emission signal at 930 nm indicates a 50 fs time constant for the Stokes shift response of P_{y-}, suggesting development of a different charge distribution in P_{y-} than that in the electronic ground state and a protein medium solvation response.

In addition to the exponential rise and subsequent decay, the pump−probe signal detected in the region of stimulated emission contains very pronounced high-frequency oscillations. The predominant modes are 140, 560, 730, and 1160 cm^{-1} as determined by LPSVD analysis and Fourier spectral analysis;

the Fourier power spectrum of the residuals after the exponential components are removed is shown as an inset to Figure 9b. The low-frequency mode is surprisingly weak, particularly in comparison with previous results.[38,41−44] The weakness of the low-frequency oscillations may result from detection on the extreme red edge of the pulse. These low-frequency oscillations are, however, prominent when detecting the transient absorption from P_{y-} near 800 nm, as shown in Figure 7.

E. Direct Excitation of P_{y+}. The dynamics associated with the upper excitonic component have been investigated by comparing transient probe transmission signals obtained following excitation at 800, 825, and 860 nm for magic-angle polarized pump−probe pulse pairs. The excitation and probing spectra are those presented in Figure 3. For the purposes of judging the relative excitation intensities, the linear absorption spectrum has been fit with four Gaussians at 760, 802, 825, and 866 nm corresponding to the transitions of H, B, P_{y+}, and P_{y-}, respectively. The overlap with each absorption band is then calculated for each pump spectrum. The 800 and 866 nm spectra overlap nearly exclusively with B and P_{y-}, respectively. However, the 825 nm excitation spectrum overlaps with all three bands in the following manner: 42% P_{y-}; 25% P_{y+}; 33% B. For each given time delay, the signals are collected for excitation with each of the pump spectra shown in Figure 3. The signal due to excitation of P_{y+} is then obtained by subtracting the appropriately scaled signals due to excitation of B and P (obtained from the 800 and 866 nm pump experiments, respectively) from the 825 nm excitation signal. The resulting signals are shown in Figure 10 for a series of time delays ranging from 50 to 500 fs. These spectra contain, to varying degrees, a large bleach component near 825 nm, a broad bleach centered at 866 nm, and a small absorption that shows up slightly below 800 nm. The time dependence of these bands is obtained by fitting the transient spectra to a series of three Gaussians, corresponding to each of the bands. This analysis shows that the 825 nm component decays with a 65 fs time constant, as indicated in Figure 10b. There is a corresponding rise in the bleach at 870 nm, while the absorption intensity remains, for the most part, the same. These data reinforce the observation of P_{y+} at 825 nm by the spectral and temporal anisotropy results of previous subsections and suggest that the internal conversion of the special ($P_{y+} \rightarrow P_{y-}$) occurs with a 65 fs time constant. The 65 fs internal conversion rate is also in agreement with the decay in the anisotropy observed after broad-band excitation of both the $P \rightarrow P_{y+}$ and $P \rightarrow P_{y-}$ transitions.

F. Excitation at 800 nm. The time, wavelength, and polarization-resolved (i.e., perpendicular and magic angle) pump−probe transients observed after excitation of B are shown in Figure 11. For clarity, the three-dimensional magic-angle data is displayed with two projections in parts a and b of Figure 11, rotated by 180° to show both the early and late time dynamics. These plots show the rapid decay of the initially prepared bleach at 800 nm corresponding to photobleaching and/or stimulated emission from B, the delayed and gradual formation of a bleach at 866 nm indicative of ground-state depletion of P, and the formation of a broad structured absorption near 800 nm that was previously identified as an excited-state absorption from P_{y-}.[38] The data does not indicate the simple decay of one band followed by the formation of another. Rather, there is a significant amount of structure, particularly at early times, in the spectral region of the $P \rightarrow P_{y+}$ transition near 825 nm. Furthermore, anisotropy measurements performed under similar conditions indicate that this wavelength region exhibits an

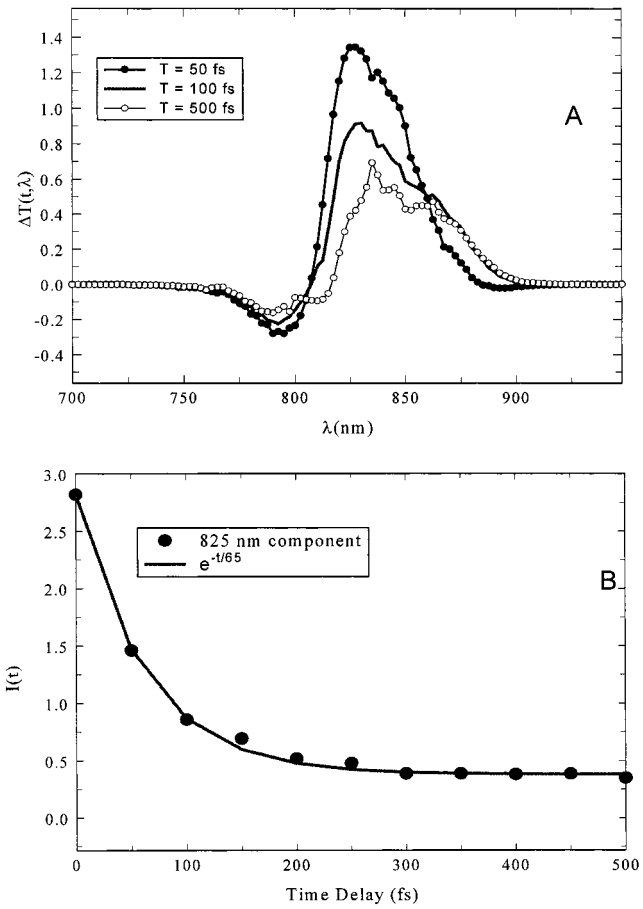

Figure 10. Direct excitation of P_{y+}. (a) Transient probe transmission spectra obtained due to excitation of the $P \rightarrow P_{y+}$ transition. Magic-angle pump−probe signals obtained following selective excitation of $B \rightarrow B^*$ and $P \rightarrow P_{y-}$ are used to isolate the dynamics due to excitation of $P \rightarrow P_{y+}$ with a pulse overlapping $B \rightarrow B^*$, $P \rightarrow P_{y-}$ and $P \rightarrow P_{y+}$. Spectra are shown for temporal delays of 50, 100, and 500 fs. (b) The spectra from panel A contain bleach/stimulated emission components at 825 and 870 nm. The decay of the 825 nm component is illustrated here. Solid circles represent the magnitude of the 825 spectral waveform obtained by fitting the experimental data. The line through the data is an exponential fit to the obtained magnitudes.

anisotropy unlike that for either the 800 or 866 nm bands due to $B \rightarrow B^*$ or $P \rightarrow P_{y-}$. The various spectrally evolving components are also observed in the perpendicular pump−probe data of Figure 11c. Here, one can see the bleach of B at 800 nm, a rapid red shifted broadening of the B band, a slower formation of the 825 nm bleach feature (P_{y+}), and the slower still formation of the P_{y-} band at 866 nm. Figure 11c is oriented to allow for a clear picture of the spectral evolution near 800 nm at early time delays. For illustration purposes, a curved arrow indicates the position of the spectrally evolving feature from 800 nm. Comparison of the relative magnitudes of the shifted component and the nonshifted feature for the magic-angle and perpendicular scans indicates that the spectral shift process involves reorientation as well as an overall red shift. This implies mixing with a state of different orientation, perhaps P_{y+}.

G. Kinetic Spectral Analysis. The wavelength-resolved pump−probe signals in this paper present a detailed description of the energy-transfer process. A meaningful fit to the data can be obtained if the following are known (or obtainable): (1) the kinetic scheme for energy transfer; (2) the spectra and relative extinction coefficients of each species involved in the energy-

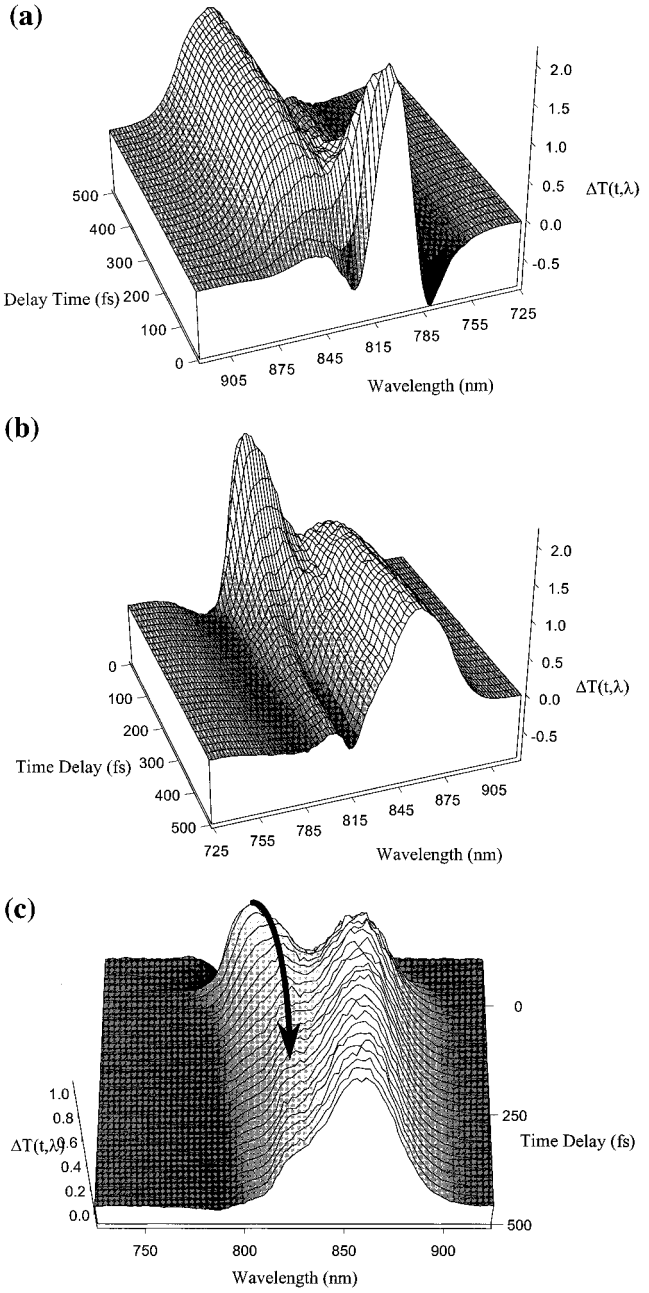

Figure 11. Entire temporal and spectral response of the photosynthetic reaction center of *Rb. sphaeroides* following excitation of the accessory bacteriochlorophyll pigments (B). Two views of the data are shown, rotated by 180° for illustration purposes. Here, a positive signal indicates a transient bleach while a negative signal indicates a transient absorption. The surface plot shows the rapid decay of a bleach at 800 nm due to B and a corresponding increasing bleach at 860 nm from P_{y-}. A smaller component at about 825 nm, between these two dominant features, can also be observed and is a associated with P_{y+}. The pump−probe relative polarization for both parts a and b is at the magic angle. (c) Time- and wavelength-resolved pump−probe data for perpendicular pump−probe polarizations. The spectra shown are for time delays ranging from −80 fs to 500 fs in steps of 20 fs. The black arrow highlights the shift in the spectral region of the accessory BChl.

transfer process; (3) the dynamics of each of the species not "directly" related to energy transfer (Stokes shifts for instance).

1. Kinetic Models. Two models are used to fit the wavelength-resolved pump−probe data. The first is a one-step kinetic model, where electronically excited B* transfers energy directly to P_{y-}. The second model invokes a two-step pathway for energy transfer, where B* transfers energy to P_{y-} by way of P_{y+}; that

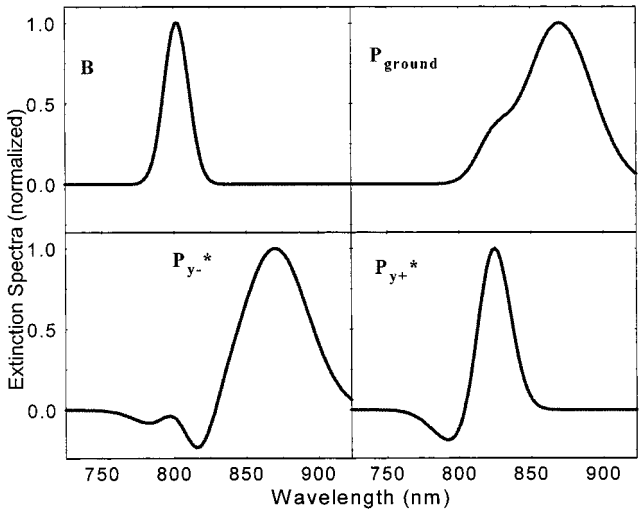

Figure 12. Spectra used for kinetic fitting of the wavelength-resolved pump−probe data. Spectra are shown clockwise from the top left-hand corner for B, P_{ground}, P_{y+}*, and P_{y-}*, respectively. The spectra are taken from experimental results and not inferred from any other source. The characteristics of each spectrum are given in the text.

is,

$$B^* \xrightarrow{k_1} P_{y-} \tag{5a}$$

$$B^* \xrightarrow{k_1} P_{y+} \xrightarrow{k_{IC}} P_{y-} \tag{5b}$$

The kinetics for each of these excited-state components, as well as their associated ground states, can be easily defined in terms of elementary kinetics.[51]

2. Effective Spectra of Electronic States. The characteristics of the spectral components associated with transitions to and from B, P_{y+}, P_{y-}, and P (ground state) bleach are shown in Figure 12. For simplicity, each spectrum is assumed to be composed of one or more Gaussian line shapes. When necessary, spectral evolution of each band is included in the model. The spectrum for B, as shown in the upper left panel, is taken to be a Gaussian centered at 800 nm, as suggested by the steady-state absorption spectrum. We have found that a rapid red shift of the 800 nm band is necessary to fit the wavelength-resolved data for early pump−probe delay times. Previous studies involving B dynamics[20] have incorporated Stokes shift processes for B, in analogy to solution results for BChl monomers.[52] However, it is not obvious that such an analogy is appropriate. For reasons that will become clear later, we will not refer to the rapid dynamics as a Stokes shift. Rather, the more general term of red shift will be incorporated. The normalized $T = 0$ spectrum for B is shown.

The upper right panel in Figure 12 shows the ground-state bleaching spectrum for P. This is composed of bands at 825 and 870 nm corresponding to P_{y+} and P_{y-}, respectively. The band positions were obtained experimentally (see the previous sections describing Figures 4, 6, 8, and 10), while the relative intensities are set by fitting both the pump probe data and the steady-state absorption spectrum. Another panel of Figure 12 shows the spectrum for the lower excitonic state of the special pair, P_{y-}. There are two parts to this spectrum, a stimulated emission component at 870 nm (at a delay of $T = 0$) and an excited-state absorption near 810 nm. The stimulated emission component undergoes a rapid Stokes shift and appears at 930 nm with a 50 fs rise time prior to decaying with the 2.8 ps charge-transfer time constant as discussed above (see Figure

9). The excited-state absorption likewise decays with a 2.8 ps time constant. These two components are treated separately in the calculations but are shown together here. Spectral evolution of any excited-state absorption from P_{y-} should occur with the same time constants as Stokes shift dynamics in the stimulated emission. Possible rapid evolution of P_{y-} absorption is not considered in this treatment. Additionally, the structure in the absorptive feature may arise from band shifts of B upon excitation of P_{y-}. As mentioned previously, all of these characteristics are considered part of P_{y-} absorption for the purposes of these calculations.

Finally, the spectrum for P_{y+}, as suggested by responses presented earlier in this paper (see Figures 4, 6, 8, and 10), is centered at 825 nm. There is a small absorption at 800 nm, as well as a tail to the red of the main peak. The origin of this absorption is not very well known. It has been suggested that there should be a transient absorption from P_{y+} to a doubly excited state of P with the spectral characteristics of P_{y-}.[20] The negative amplitude feature observed here might be a result of competition between a narrow stimulated emission band at 825 nm and a broad absorption band further to the red. This effective spectrum for P_{y+} and its justification through kinetic spectral analysis is one of the important new results of this paper.

In the kinetic analysis, the spectra for each of these components are assigned to the relevant step of the kinetic framework. The magnitude of each feature's extinction coefficient is allowed to vary with respect to the extinction coefficient of B, i.e., the initially excited population. One of the tests for validity of a particular kinetic scheme will be the ability to reproduce the extinction coefficients as indicated in the linear absorption spectra and other pump−probe data presented in this paper.

3. One-Step Mechanism. The first model invoked to simulate the experimental data is one-step energy transfer from B to P_{y-} using the kinetic scheme mentioned above and the spectra presented in Figure 12, with the exception of P_{y+}. As a first approximation, the Stokes shift for B was considered to be 190 cm^{-1}, consistent with the Stokes shift observed in ether solutions of monomeric bacteriochlorophyll *a*.[53] This model adequately reproduces the decay of the bleach at 800 nm due to B, as well as the rise of the bleach at 870 nm, but fails to reproduce the significant amount of structure at 825 nm.

A much better fit to the magic-angle data is obtained if the Stokes shift for B is allowed to increase from the ether solution value. Use of a Stokes shift of 260 cm^{-1}, an exponential "Stokes shift" time of 20 fs, and a rate constant of $(1/k_1) = 120$ fs, yields a good fit. Although the magic-angle data is fit well using this model, the amplitudes of each component must be adjusted dramatically to fit the full time and wavelength-dependent anisotropy data. In particular, the anisotropy associated with the spectrally shifted portion of "B" had to be reduced from the *B* value of 0.4. This model also fails to account for the 65 fs decay of the 825 nm spectral component shown in Figure 10.

4. Two-Step Mechanism. The second model for energy transfer postulates a two-step energy-transfer mechanism, whereby the upper excitonic state of the special pair serves as the intermediate between B* and P_{y-}. Using the kinetic scheme of eqs 5a and 5b and the spectra in Figure 12, a good fit is obtained to the entire wavelength-dependent data as shown in Figure 13. The full spectral data, as well as the fit, for a series of time delays is shown in the panels of Figure 13. The best fit is obtained with time constants of 120 and 65 fs and a red shift magnitude for B of 260 cm^{-1} (190 cm^{-1} = Stokes shift value for ether solution[53]). The data for temporal delays of 100 and 160 fs also indicate the amplitudes and spectral positions of the contributing spectral components from Figure 12 plus the red shift stimulated emission band associated with B. Note that the amplitude for the 800 nm component and the red-shifted feature have identical amplitudes and temporal decay characteristics. The magnitude of the red-shifted band is important for the determination of the origin of this feature. Also, the individual spectral components as shown for pump−probe delays of 100 and 160 fs are convoluted with the pulse spectrum.

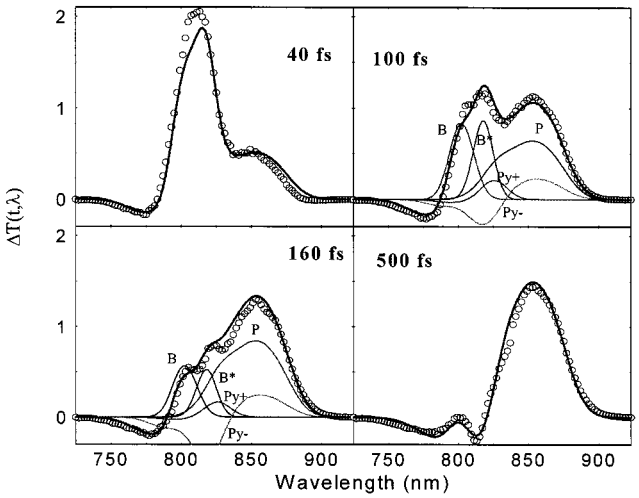

Figure 13. Kinetic analysis of the wavelength-resolved magic-angle pump−probe spectra obtained after excitation at 800 nm. The model consists of a two-step energy-transfer mechanism, $B \rightarrow P_{y+} \rightarrow P_{y-}$, where the two steps occur with $k_1 = 120$ fs and $k_{IC} = 65$ fs time constants, respectively (where IC refers to internal conversion of P), and the spectra for each species are experimentally determined. Fits to wavelength-dependent transients using the spectra presented in Figure 12 and a two-step kinetic scheme are given. The open circles represent the experimental data, while the lines indicate the kinetic fit. The individual spectral contributions from B, B*, P_{y+}, P_{y-}, and P ground state are shown in the 100 and 160 fs delay time spectra.

Figure 14 is a temporal representation of the kinetic model analysis for a few detection window data sets ($\lambda_d = 800$, 825, and 865 nm). The solid lines through the data points indicate the fit using the two-step model of eq 5b. The agreement is very good. It should be pointed out that the vertical scales in Figures 13 and 14 are the same. Furthermore, the rapid rise kinetics of the $\lambda_d = 825$ nm data in Figure 14 results primarily from the influence of the B* red-shifted component and the decay dynamics reflect both the $B^* \rightarrow P_{y+}$ and $P_{y+} \rightarrow P_{y-}$ excitation transfer steps.

In addition to the spectral responses detected in the region of the Q_y absorption bands, the kinetic models can be tested by their ability to duplicate the rise in stimulated emission from P_{y-}. Figure 15 shows the pump−probe signal obtained by pumping B with narrow band pulse and detecting the probe response at the stimulated emission wavelength (930 nm). The rise dynamics predicted by the two-step model and the one-step model, both incorporating a large red shift for B*, are also shown. The rise in the stimulated emission is better reproduced by the two-step mechanism (solid line), which yields a slightly slower rise than does the one-step transfer rate (dashed line). In both cases, the subsequent decay is modeled with a single-exponential component corresponding to the charge-transfer time ($\tau = 2.8$ ps). The presence of a substantial 2.8 ps decay indicates that the pump−probe measurement is indeed sensitive to emission from P_{y-}, not simply ground-state bleach terms.

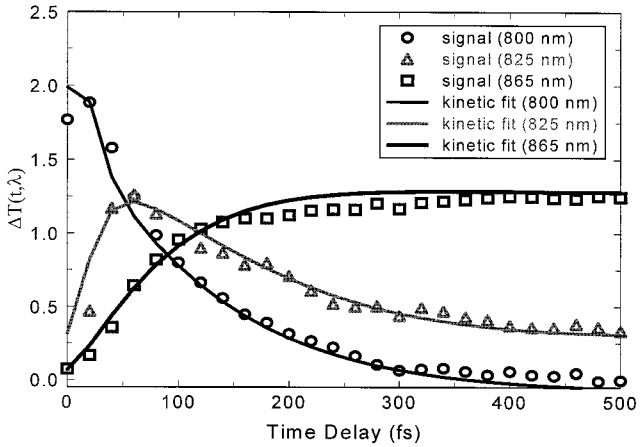

Figure 14. Temporal fit to the wavelength-resolved transients. Experimental data (symbols) and the calculated fits (solid lines) are shown for 800, 825, and 865 nm. The fit is obtained from the two-step model for energy transfer, $B^* \rightarrow P_{y+} \rightarrow P_{y-}$, with time constants of 120 and 65 fs for the two steps. The spectra used for each individual component are indicated in Figure 12. The calculated time- and wavelength-resolved signals are convoluted with the instrument response function both in the temporal and spectral domain accounting for both the finite temporal and spectral resolution. The lines represents the total calculated amplitude for the three wavelengths examined, 800 nm, 825 nm, and 865 nm. The units along the vertical axis are the same as for Figure 13.

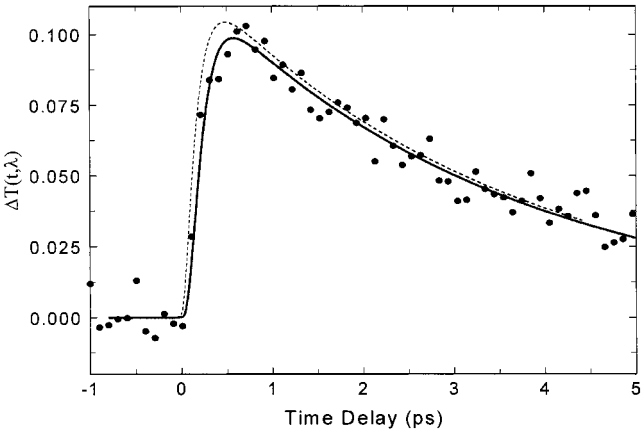

Figure 15. Stimulated emission from P_{y-} after excitation at 800 nm detected via wavelength-resolved pump−probe. The solid circles are the experimental data points, while the solid line is the kinetic fit to the data incorporating a two-step energy-transfer scheme with the time constants indicated previously, as well as a 50 fs Stokes shift for P_{y-}*. The dashed line is the stimulated emission transient predicted by a one-step model with a 120 fs energy-transfer time and a 50 fs Stokes shift for the special pair.

For both models, the relative extinction coefficients of the various components were varied to obtain an acceptable fit to the experimental results. The resulting coefficients for the one-step pathway and the two-step pathway for energy transfer are given in Table 2, as are the coefficients obtained by fitting the

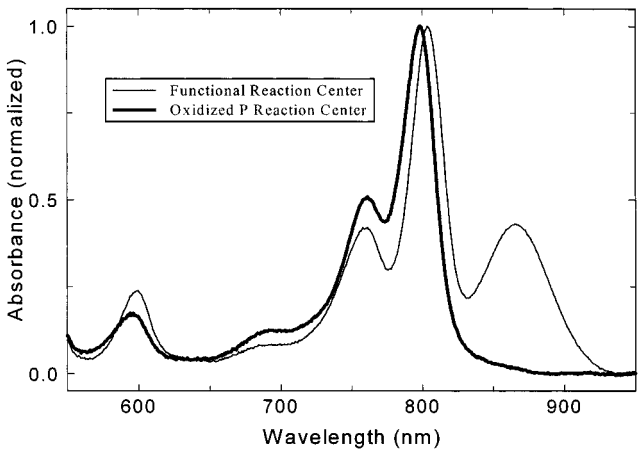

Figure 16. Comparison of the linear absorption spectra for functional reaction centers (light line) and reactions centers with chemically oxidized special pairs (dark line). Oxidization of P is obtained by the addition of $Fe^{III}(CN)_6$. Depletion of the optical band at 865 nm in the oxidized sample indicates that greater than 95% of the special pair dimers within the sample are oxidized.

linear absorption spectra and also the pump−probe spectra obtained for excitation at 870 nm (Figures 5 and 6). The ability to reproduce a consistent set of extinction coefficients is a test of the validity of the model. The two models differ in their extinction coefficients for P_{y-} (S.E.) and ground-state bleaching of P. Of the two models, the two-step mechanism agrees more precisely with the linear absorption spectrum values. The ability of the two-step model to reproduce the detailed time- and wavelength-resolved spectra, the rise in stimulated emission from P_{y-} at 930 nm, and steady-state absorption coefficients strongly suggests that a multiple-step mechanism is active in the RC.[20]

5. Chemically Oxidized Special Pair and High-Fluence Conditions. The rapid dynamics observed in Figure 11 change dramatically upon oxidation of the special pair. Oxidation of the special pair is obtained by the addition of an excess of $Fe(CN)_6$ to the reaction center samples, a procedure that results in oxidation of greater than 95% of the special pairs within the sample. The absorption spectrum for the chemically oxidized reaction centers (P^+BH) is shown in Figure 16, in comparison with the functional reaction centers (PBH). The lack of absorption associated with the transition into the P_{y-} band at 870 nm indicates the extent of oxidation is at least 95% effective. In addition, the spectrum shows reduced absorbance near 825 nm consistent with the absence of the $P \rightarrow P_{y+}$ transition. Finally, the absorption band for B is blue shifted with respect to the functional RC absorption peak, while H remains unaffected. The blue shift might be an electrochromic shift due to the presence of the positively charged special pair. Alternatively, the B spectrum may shift toward higher energy due to absence of coupling with the special pair excitonic states.

Figure 17 shows the time- and wavelength-resolved pump−probe magic-angle polarization signals detected under exactly

TABLE 2. Kinetic Model Analysis[a]

spectral component	one step	two steps	excitation at 870 nm	linear absorption spectrum
P_{y-}* (S.E.)	0.32	0.49	∼0.43	NA (∼0.43)
P_{y-}* (absorption)	0.279	0.27	0.16	NA
P_{y+}	NA	0.24	0.09	0.098
P (ground-state bleach)	0.392	0.44	0.43	0.43

[a] The extinction coefficients predicted from fitting energy transfer data via one-step mechanisms and two-step mechanisms, excitation at 860 nm data, and the linear absorption spectrum. All extinction coefficients are listed in comparison with that of B, which has been set to unity. The values reported are peak extinction coefficients, not integrated oscillator strengths.

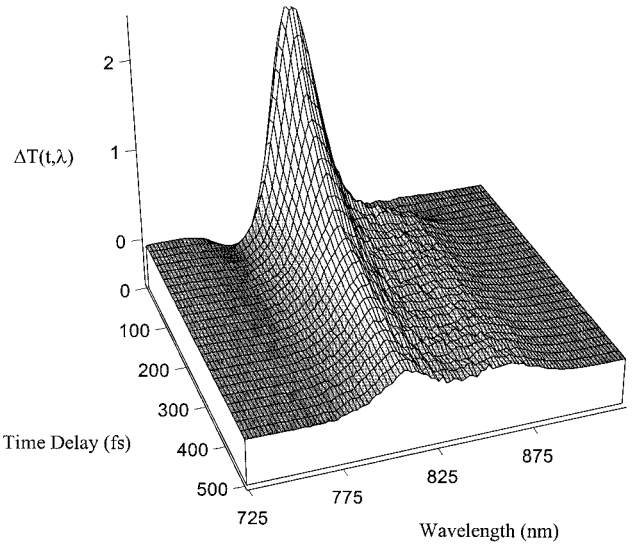

Figure 17. Entire temporal and spectral response of the chemically oxidized photosynthetic reaction center of *Rb. sphaeroides* following excitation of the accessory bacteriochlorophyll pigments termed B. The surface plot shows a relatively slow decay of a bleach of B at 800 nm but no significant rise at 870 indicating the absence of formation of P_{y-}*.

the same conditions as those used in Figure 11 but with an oxidized special pair. With this sample, an initial bleach is prepared at 800 nm that decays with a 300 (±50) fs time constant, in contrast to the <100 fs decay observed for a functional RC. In additional, there is only a minimal rise in the signal at 860 nm and no transient absorption. The minimal rise probably reflects the small population of nonoxidized reaction centers in the sample. Note the absence of spectral shifting behavior of the 800 nm bleach/stimulated emission feature that was evident in Figure 11 for functional RC's. The combination of the data sets presented in Figures 11 and 17 indicates that the excited accessory bacteriochlorophyll, B*, undergoes energy transfer to a healthy (neutraly charged) special pair but, upon oxidation of the special pair, B decays via some other mechanism. Furthermore, the 300 fs decay time observed here is the same as one component in pump−probe data obtained for high-fluence excitation.

An example of a high-fluence pump−probe signal with both excitation and detection at 800 nm is shown in Figure 18. An adequate fit of the data (solid line) in Figure 18 requires three exponential components, 100 fs, 308 fs, and a static component on the 0−1 ps time scale. The intermediate component is eliminated under the fluence conditions used for all other data presented above. The fast decay is the B* → P_{y+} excitation-transfer step, while the static component likely reflects the electrochromic shift of B that occurs in this spectral region in association with the formation of the charge-separated product P^+BH^-. In the data window of Figure 18, the time scale for this process is not well determined. The amplitude of the 300 fs component, the same time constant as in the oxidized reaction center, is fluence dependent, corresponding to the fraction of doubly excited accessory bacteriochlorophyll reaction centers in the sample.[20]

6. Electronic Coherence. Excitation of multichromophoric systems with short-duration (transform-limited) pulses can produce electronic state coherences in addition to vibrational coherences. These electronic coherences are selectively detected in the anisotropy signal as shown in Figure 8. Another optical coherence can be established between the H and B transitions using pump and probe pulses centered at 760 nm; the resulting

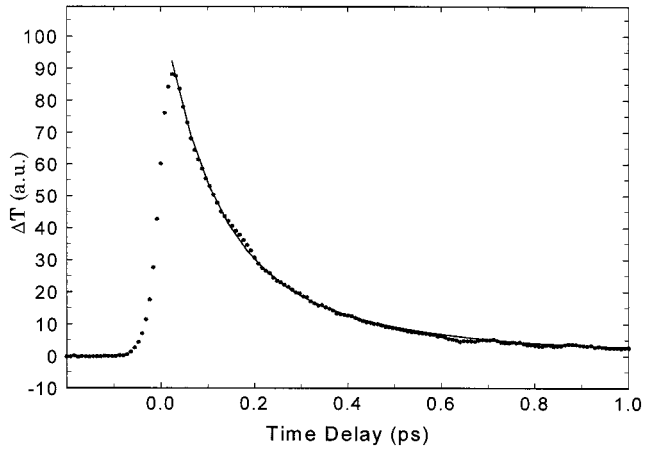

Figure 18. Pump-induced probe transmission transient obtained under high-fluence excitation conditions. The solid circles indicate experimental pump probe data with excitation and detection at 800 nm. Relatively high repetition rate (100 kHz) pulse trains and tight focusing result in both multiple excitation of reaction centers with each laser pulse and excitation of charge separated reaction centers. Two exponential components with time constants of $\tau_1 = 100$ fs (69% amplitude), $\tau_2 = 308$ fs (29%) and a constant offset of 2% were necessary to fit the data.

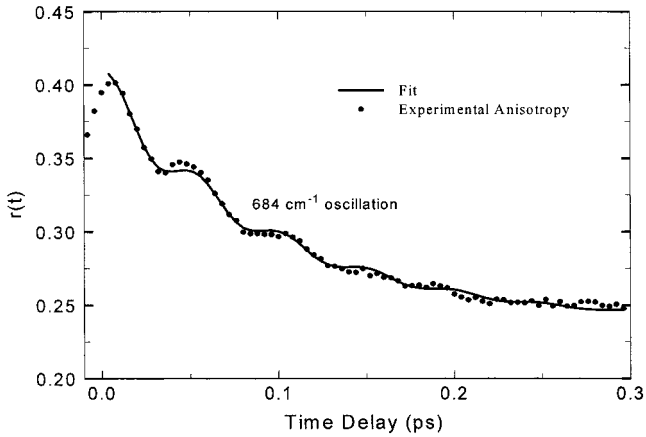

Figure 19. Time-dependent anisotropy observed after excitation of the B and H bands of the photosynthetic reaction center. The solid circles represent the experimental data, while the solid line is a fit with the following model: $f(t) = a\exp(-t/\tau_1) + b\cos(\omega t + \varphi)\exp(-t/\tau_2) + c$ with values of $a = 0.162$, $\tau_1 = 96$ fs, $b = 0.016$, $\omega = 684$ cm^{-1}, $\tau_2 = 88$ fs, $\varphi = -0.92$ rad, and $c = 0.23$.

anisotropy signal is shown in Figure 19. The observed 684 cm^{-1} oscillation corresponds to the H−B splitting in the steady-state spectrum of Figure 1. Interestingly, the 96 fs decay observed in this anisotropy measurement is identical to the difference in time scales for the B* → P* (147 fs) and H* → P* (257 fs) energy-transfer pathways as measured by Stanley et al.[23]

IV. Discussion

A. P_{y+} Spectral Position and Internal Conversion of P*. The measurements presented in this paper provide experimental parameters describing the characteristics of the excitonic splitting on the special pair, particularly the energies of the two excited states, P_{y+} and P_{y-}, the angle between the two associated optical transition dipole moments, and the ratios of the integrated intensities. These observations are considered in terms of simple excitonic theory, which describes the interaction of two molecules forming a dimer.[54,21] Within this theory, the first excited state of the dimer is split into two excitonic states, formed by either symmetric or asymmetric linear combinations of the monomer transitions. The energies of the excitonic states

TABLE 3. Excitonic Model Analysis with Spectral Inhomogeneity

	ratio of P_{y+} to P_{y-} transition dipole strengths (D_+/D_-)			
variable parameter	$\sigma = 0$	$\sigma = 100\ cm^{-1}$	$\sigma = 200\ cm^{-1}$	$\sigma = 300\ cm^{-1}$
ω_{L^*M} and ω_{LM^*}	0.197	0.203	0.223	0.251
$^1/_2(\omega_{L^*M} + \omega_{LM^*})$	0.197	0.197	0.197	0.197
U	0.197	0.225	0.418	0.788
experimental value	0.10 ($\pm$0.03)			

become

$$\omega_+ = \frac{\omega_{L'M} + \omega_{LM'}}{2} + \frac{U}{\sin\alpha} \tag{6a}$$

$$\omega_- = \frac{\omega_{L'M} + \omega_{LM'}}{2} - \frac{U}{\sin\alpha} \tag{6b}$$

where $\omega_{L'M}$ and $\omega_{LM'}$ are the transition frequencies for the P_L or P_M monomers constituting the special pair. The resonance integral between the two monomers, U, is usually taken to reflect the dipole−dipole interaction, although the close proximity of P_L and P_M suggests that more terms need to be considered.[19] The angle α, used for mathematical simplification, is determined by the resonance integral U and the difference between the two monomer transition frequencies ($\omega_{L'M} - \omega_{LM'}$); that is,

$$\tan\alpha = \frac{2U}{\omega_{L'M} - \omega_{LM'}} \tag{7}$$

The dipole moments for the two excitonic transitions depend only on the value of α and the orientation of the monomer Q_y transitions for P_L and P_M (μ_L and μ_M); that is,

$$\mu_+ = \cos\left(\frac{\alpha}{2}\right)\mu_L + \sin\left(\frac{\alpha}{2}\right)\mu_M \tag{8a}$$

$$\mu_- = \sin\left(\frac{\alpha}{2}\right)\mu_L - \cos\left(\frac{\alpha}{2}\right)\mu_M \tag{8b}$$

The transition dipole directions can be obtained from the crystal structure for the RC. Finally, the ratio of the transition dipole strengths is given by

$$\frac{D_+}{D_-} = \frac{1 + \sin\alpha\cos\theta}{1 - \sin\alpha\cos\theta} \tag{9}$$

where θ is the angle between the two monomer Q_y transitions.

If the transition frequencies for the individual monomer transitions are identical, i.e., $\omega_{L'M} - \omega_{LM'} = 0$, then $\alpha = \pi/2$. This leads to the prediction that the excitonic state transition moments are perpendicular to each other and that the ratio of dipole strengths is 1:7.5. This is not in agreement with the present experimental results (70°, ratio of 1:10) and those from low-temperature linear dichroism and hole-burning results, which indicates that the angle between the two excitonic states is 70° rather than 90° and the ratio of dipole strengths is 1:8.

Taking the experimentally determined anisotropy for P_{y+} of −0.05 listed in Table 1, it is possible to determine the angle α and the relative contributions of μ_L and μ_M to the two excitonic states. For this anisotropy value, α is approximately 62°, implying that P_{y+} is composed mostly of P_L whereas P_M contributes more to P_{y-}. Under these conditions, the resonance integral, U, is 276 cm^{-1}, while the difference in transition frequencies $\omega_{L'M} - \omega_{LM'}$ is 294 cm^{-1}. Although these numbers give a reasonable representation of the energies and the relative orientations of the excitonic states, the ratio of dipole strengths is approximately 1:5, rather than the experimentally observed 1:10. Hence, the experimental results are not reproduced by a simple excitonic coupling model including only the special pair, allowing for (environmentally induced) asymmetries in the monomer transition frequencies.

The relative magnitudes of the P_{y+} and P_{y-} transition moments may be influenced by an inhomogeneous distribution of special pair transition frequencies. The contribution of inhomogeneity to the P_{y-} excitonic band has recently been characterized at room temperature via photon echo experiments;[27] the contribution is found to be significant. A distribution of donor energy levels (i.e., P_{y-}) is also thought to give rise to nonexponential electron-transfer dynamics observed through stimulated emission from P_{y-}.[55] Inhomogeneity in the special pair excitonic levels can arise from uncorrelated distributions in the site (monomer) transition frequencies, ω_{L^*M} and ω_{LM^*}, center frequencies, $^1/_2(\omega_{L^*M} + \omega_{LM^*})$, or the P_L-P_M coupling strength, U. The effect of these three sources of inhomogeneity on the energy levels obtained using eqs 6−9 was explored in the following way. A distribution in site transition frequencies was incorporated into the calculation by randomly selecting ω_{L^*M} and ω_{LM^*} from two independent distributions (normal distribution, standard deviation = σ) and calculating the ratio of P_{y+} to P_{y-} transition dipole strengths for 10^4 pairs of frequencies. Likewise, inhomogeneity due to distributions of $^1/_2(\omega_{L^*M} + \omega_{LM^*})$ or U was modeled by the selection of random values for each of these parameters. The average difference in transition frequencies between the two monomers, the coupling strength, and the center frequency are kept the same as the values listed in the previous paragraph, which described the energetics without considering broadening mechanisms. The effect of inhomogeneity on the ratio of dipole moments is illustrated in Table 3 for all three types of inhomogeneous distributions discussed here; the results are listed for three successively increasing distribution widths for each parameter. A finite distribution of either the site energies or the coupling strength increases the transition dipole strength of P_{y+} with respect to P_{y-}, while variation of the center frequencies has no effect on the average dipole ratio. The magnitudes listed in this table correspond to the average ratio obtained after 10^4 calculations. These types of inhomogeneity only serves to cause further deviations from the experimental result.

It is possible that the disagreement between the model and the anisotropy results presented in this paper may be resolved by considering interactions between the special pair BChl's and the other chromophores in the reaction center. In this delocalized states picture the observed optical bands correspond to excitation into energy levels resulting from excitonic interaction of all pigments. Haran et al.[19] found the consideration of delocalized states necessary to reproduce their experimental results; the most promising model was an adaptation of the delocalized state Hamiltonian of Scherer and Fischer[56,13] that includes dipole−dipole coupling between chromophores and also considers charge-transfer states of the special pair. Haran et al.[19] found that increasing the coupling between the two accessory BChl's (i.e., B_L and B_M) and the charge-transfer states of the special pair from the value put forth by Scherer and Fischer improved

agreement with experiment, although the authors concluded present delocalized state models provide an inadequate description of the reaction center dynamics. Discussion on the point of delocalized states will continue in subsection C below.

B. Stokes Shift Dynamics of P_{y-}. The rapid Stokes shift observed for the special pair can be used to gain information about the transition frequency correlation function, which is useful for calculating electron-[57] and energy-transfer times, as well as elucidating cofactor−protein interactions. The transition frequency correlation function M(t) is defined as[58,59]

$$M(t) = \frac{\langle \omega(t)\, \omega(0) \rangle}{\langle \Delta\omega^2 \rangle} \tag{10}$$

where $\omega(t)$ is the electronic transition frequency at a time t after excitation. In the high-temperature limit, $M(t)$ becomes equivalent to the Stokes shift correlation function:[60]

$$S(t) = \frac{\nu(t) - \nu(\infty)}{\nu(0) - \nu(\infty)} \tag{11}$$

which can be evaluated using fluorescence up-conversion[61,62] data or, as in the present case, stimulated emission spectra obtained as a function of pump−probe time delay.

The data shown in Figure 9 were well fit with a model function incorporating a 50 fs exponential Stokes shift, implying that $M(t)$ also contains a 50 fs component. Another paper[27] that describes the results of photon echo measurements on the special pair shows that the time shift of the integrated photon echo maximum as a function of population delay time (which approximately follows $M(t)$[59,63]) contains a rapid decay of 50 fs or less, in good agreement with the Stokes shift results from Figure 9. The Stokes shift observed here for the special pair P_{y-} state is both larger and faster than any shift observed for BChl monomers in solution, which are generally on the order of 200 cm^{-1} and occur on a few picosecond time scale.[52] The fast excited-state relaxation most likely results from three processes,[38] internal vibrational dynamics, strong coupling to the phonon bath, and mixing with states containing large charge-transfer character.[13]

The observation of coherences corresponding to vibrational modes with frequencies up to 1160 cm^{-1}, in addition to the low-frequency modes observed here and elsewhere,[38,41−44] indicates that the vibrational contribution to $M(t)$ is significant, a conclusion that is well supported by photon echo measurements.[27] The data of Figure 9 is the first report of such impulsively prepared high-frequency oscillations in the photosynthetic reaction center; these modes have, however, been observed in resonance Raman measurements.[64] A more systematic report of the vibrational coherences prepared in association with the optical transitions from H, B, and P will be reported elsewhere.[65]

Relaxation of P_{y-} is also facilitated by electron−phonon coupling to the protein environment. Hole-burning results for the photosynthetic reaction center have shown that BChl and other cofactors within photosynthetic proteins are typically coupled to a distribution of low-frequency (20−30 cm^{-1}) acoustic phonons.[66] The strength of this coupling was found to depend greatly on the biological function of the cofactor under investigation. The weak coupling of BChl monomers and dimers in the light-harvesting antennas[66,67] is contrasted by very strong coupling for BChl molecules in the reaction center, particularly the special pair.[66] For the special pair, this electron−phonon coupling and a strongly displaced intradimer vibrational mode, termed the "marker mode", combine to yield a low-temperature reorganization energy of 230 cm^{-1} at 10 K.[66,68,69,70,71] The rapid decay in $M(t)$ observed in both pump−probe and photon echo measurements indicates that the phonon band coupling to the special pair at room temperature is both broad in frequency and very strong. The spectral density obtained from three pulse photon echo measurements indicates that the effective phonon spectral density has magnitude even at frequencies as large as 2000 cm^{-1}.[27]

Recently, Marchi et al. have calculated the P−P* energy gap correlation function via molecular dynamics simulations.[72] The resulting correlation function for an RC complex at 50 K shows a fast decay that is complete by 500 fs. The time scale is slightly longer than that predicted by the present Stokes shift measurement or photon echo studies performed at room temperature. Both the BChl dimer and the protein bath contributed significantly to the decay in $M(t)$, the former of which exhibits significant oscillatory behavior. The simulations, however, do not model a charge-separation process in the special pair that precedes the charge-transfer process to adjacent B and H chromophores.

C. Spectral Evolution of "B*". The time-dependent spectra obtained after 800 nm excitation and shown in Figure 11 indicate that the initially prepared excited state (termed B*) undergoes rapid spectral evolution prior to and during energy transfer. This process is included in the kinetic analysis by simply allowing the spectrum for B*, shown in Figure 12, to shift toward longer wavelengths as a function of time. Invoking a rapid red shift (20 fs time constant) of 260 cm^{-1} allows for a good fit to the data, although the origin of this shift is not known. One possibility is that the spectral evolution corresponds to a rapid Stokes shift of the accessory BChl, similar to those observed for other biological systems.[73,74] (It should be noted that neither the magnitude nor the time scale for a rapid Stokes shift of B* has been previously established through experimental studies; it may be very difficult to measure via conventional techniques due to the short lifetime of the excited state). The time scale and magnitude of the B* Stokes shift in the reaction center protein is most often approximated by the values observed for monomers in solution, where Stokes shift magnitudes of approximately 200 cm^{-1} are observed on a few picosecond or longer time scales.[52] The assignment of the rapid spectral evolution to a dipolar solvation process seems unlikely, however, in light of the absence of such a shift in the pump−probe results for reaction centers where P has been oxidized by the addition $Fe^{III}(CN)_6$ (see Figure 17). In this latter case, the signal obtained after excitation of B remains peaked at 800 nm for the lifetime of the signal. If the shift observed in the functional RC's is due simply to excited-state relaxation or solvation dynamics of B* accompanied by bath reorganization and internal vibrations, it should also appear in the oxidized samples. It is possible that oxidization of the special pair affects the chromophore−bath coupling of B in such a way that solvation-type dynamics are suppressed, although this seems unlikely. Furthermore, the echo measurements indicate no discernible difference in the two-pulse echo signals for B in functional or oxidized samples.[27]

The observation that we are compelled to make suggests that the ultrafast B* red shift in functional reaction centers is intricately related to the energy-transfer process; a proper understanding of this evolution may yield valuable insights into the mechanisms of energy transfer. Two possibilities for energy transfer related origins of the spectral dynamics will be discussed, asymmetric kinetic energy-transfer rates from spec-

trally distinct B molecules to P_{y+} and coherent energy-transfer mechanisms between B* and P_{y+}.

An apparent red shift in the time- and wavelength-resolved pump−probe signal obtained after excitation of B may result from asymmetric kinetic energy transfer rates from B_L and B_M to the special pair. This can be seen if the optical transitions into B_L* and B_M* occur at slightly different energies; energy transfer occurring with a higher rate from the high-energy B* level would preferentially deplete the blue edge of the spectrum, and the net bleach or stimulated emission band will appear to shift toward the red. In contrast, rapid energy transfer from the low-energy B* would be exhibited by an apparent blue shift. Information about the difference in energy-transfer rates between the B* states of higher or lower energy can be gleaned from careful inspection of high-fluence data, where both B_M* and B_L* are excited in the same reaction center.

Recent work from van Grondelle's group on mutant and wild-type sphaeroides reaction centers[24−26] has indicated another pathway for electron transfer not involving the special pair directly. They suggest that B* can convert to B^+H^- in a few hundred femtoseconds. Calculation of the optical fluence employed in their study (∼20 pJ/(μm^2)) indicates that both accessory bacteriochlorophyll *a* chromophores were excited in a large fraction of the irradiated reaction centers in the ensemble. Hence, whereas one of the two B* chromophores could decay via the normal channel described in this paper producing P_{y-} (which in the case of the YM210W mutant did not create charge-separated products P^+BH^-), the second B* would be forced to decay through some other channel. Van Grondelle's group suggested a direct decay to PB^+H^-.[24−26] Furthermore, the transient probe transmission spectra in that report (Figure 4 of ref 25) showed a greater depletion on the red edge of the B band (at early delay times), indicating that the bluer absorbing accessory bacteriochlorophyll *a* decays more slowly, a fact that does not allow the interpretation of the fast Stokes shift of B due to the existence of two distinct B* → P_{y+} transfer rates.

The pump−probe signal for chemically oxidized reaction centers after excitation at 800 nm exhibits decays nearly 3 times slower than that observed for healthy reaction centers. This intermediate time scale decay is the same as that observed for high-fluence data (see Figures 17 and 18). In the case of the high-fluence data, the decay may be due to the relaxation of the second excited accessory bacteriochlorophyll *a* cofactor whose energy transfer is blocked by the earlier energy transfer to the special pair from the other B cofactor. Hence, the prompt decay of the signal would correspond to the B* → P_{y+} energy transfer, while the ∼300 fs component, which is the same time constant observed for the oxidized reaction center sample, corresponds to another channel for nonradiative decay of the second excited accessory bacteriochlorophyll. Furthermore, the approximately 300 fs decay of B* in the oxidized reaction center sample examined here may decay, by similarity of time scale with van Grondelle's work, to B^+H^-. No identifiable spectroscopic feature that would indicate B^+H^- appears on a 300 fs time scale however. Further studies of the chemically oxidized system will be undertaken to spectrally identify the final state for relaxation of B* excitation.

Recent work from the Boxer group[23] has addressed the issue of asymmetric energy-transfer rates within both wild-type and β-mutant (M)L2144 reaction centers of *Rb. sphaeroides*. The mutant reaction center contained a bacteriochlorophyll *a* (β_L) in place of the bacteriopheophytin along the L branch of the RC, resulting in a distinct band in the absorption spectrum near 780 nm. Excitation could then be placed either on the L (β_L) or the M side (H_M) through excitation at 781 nm or 759 nm. The resulting energy-transfer rates β* → B_L* → P* or H* → B_M* → P* were comparable, with the β_L route appearing to be slightly faster. The similarity in these rates implied that the B_L* → P* and B_M* → P* energy transfer pathways exhibit similar rates.[23]

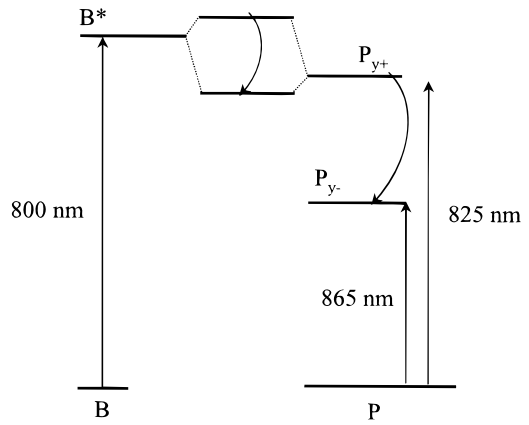

Figure 20. Schematic for delocalized states picture emphasizing the coupled states representation for B* and P_{y+} and the subsequent excitation-transfer processes. Coupling of the reaction center pigments results in delocalized states.

The Aartsma group[75] has also discussed the possibility of unequal energy-transfer rates from B_L* and B_M* to the special pair through pump−probe techniques. These experiments observed the decay of the 800 nm band following 800 nm excitation of both native and modified reaction centers from *Rb. sphaeroides*. In this case, the modified reaction center solutions contained sodium borohydride, an agent that serves to shift the absorption of B_M to 765 nm. The 800 nm excitation then populated only B_L* for the modified RCs, as opposed to both B_L* and B_M* for native reaction centers. They found that differences in the decay rates of the 800 nm band observed for the two samples were within the reported error in the experiment. In other words, the energy-transfer rate observed from B_L* to P was the same as the observed rate when B_L* and B_M* were equally prepared, implying that both accessory bacteriochlorophylls have the same energy-transfer rates.[75] This study is in agreement with the findings of the Boxer group[23] and the calculations of Haran et al., who found that the (Förster) energy-transfer rates from B_L and B_M to the special pair were similar (B_M, 130fs, B_L, 158fs).[19]

The second and more interesting origin for the spectral dynamics observed during energy transfer arises from coherent interactions between B* and P_{y+}. The prospect of coherent energy transfer has been presented before. Jonas et al.[20] suggested that coherent mechanisms may be active in the reaction center based on disparity between the observed rates and those predicted using Försters theory.[21] Strong coupling or electronic mixing between the accessory BChls and a neutral special pair may result in delocalized states that have their own spectral and temporal characteristics. In this picture, the spectral evolution observed after excitation at 800 nm represents movement along a delocalized coordinate.

The rapid excited-state spectral evolution discussed above is not accompanied by a concomitant recovery in the ground-state bleach; this later process occurs with a ∼120 fs time constant. This suggests a type of excitonic coupling between B* and P* that is different than that for the ground-state species. This scheme is illustrated in Figure 20, where the B* and P_{y+} "zeroth-order" states are coupled and form mixed character delocalized

states. The rapid (20 fs) red shift of B* can then be understood as resulting from the coherent oscillation of the excitation between the upper and lower delocalized states, and the 120 fs transfer rate in the kinetic model reflects the population relaxation between these states forming the "zeroth-order" P_{y+} state.

The practicality of any explanation for excitation transfer involving coherent mechanisms hinges on the rate of electronic dephasing between the relevant excited-state electronic levels. In this framework, the excitation can be thought of as oscillating between the two states involved in the energy-transfer dynamics;[21] the oscillation frequency corresponds to the energy gap between the energy levels. In the absence of electronic dephasing or other damping mechanisms, the oscillations will continue indefinitely. If dephasing and damping mechanisms are present and of the appropriate time scale, then it is possible for the coherent oscillation to be effectively halted after half a period, resulting in a rapid and efficient energy transfer between the states. If we consider the energy difference between the B* and P_{y+} mixed states to be 380 cm^{-1} (corresponding to 800 nm and 825 nm optical transitions), then a half period of the excitation oscillation would occur in 44 fs. Electronic dephasing between the B* and P_{y+} levels must occur rapidly enough to avoid return transfer to the B*-like delocalized state (88 fs full period) yet slowly enough to allow for coherent evolution to P_{y+}. The time domain anisotropy results for the special pair presented in Figure 8 imply that electronic coherence between P_{y+} and P_{y-} decays with a $\tau = 35$ fs exponential time constant. This coherence decay rate for exciton levels of mostly P character was significantly faster than that indicated by similar experiments on the B and H bands of the reaction center (88 fs decay) or the B820 dimeric subunit from LH1 where excitonic state coherence decayed with $\tau = 80-100$ fs exponential decays.[50] The decay of electronic coherence between B* and P_{y+} must be of a time scale similar to or faster than that for the $P_{y+}-P_{y-}$ coherence to prevent any significant return transfer. If an analogy is drawn between the electronic dephasing rate between excited energy levels and the electronic dephasing rates for ground−excited-state optical coherence observed through photon echos, then excited-state coherences involving B* should decay faster than those involving P_{y-}. Two pulse photon echos B and P_{y-} decay with exponential time constants of 10 and 11.5 fs, respectively. Furthermore, the dephasing rates observed via two-pulse photon echos for of $0-i$ transitions are substantially faster than the dephasing rates observed through anisotropy measurements for $i-j$ coherences, where i and j represent two different excited states. This suggests that the fluctuations of the individual excited-state energy levels (i and j for instance) within the reaction center are correlated to some degree, rather than being completely random. These considerations suggest that coherences may exist in the reaction center over the appropriate time range to allow energy transfer through coherent evolution.

Coherent evolution involving B* and P_{y+} should be observable in careful anisotropy measurements in the 800−830 nm spectral range. Preliminary evidence of oscillations in the anisotropy similar to those shown in Figures 8c and 19 suggests that such a coherence exists. However, it should be pointed out that the appearance of such oscillations could also occur between energetically close lying electronic states that do not share a common ground state (as in Figure 19) and are not necessarily electronically coupled to each other. Associated studies of the evolving "location" of the excitation must also be established.

V. Conclusions

The experimental results presented in this paper warrant a number of conclusions that are of relevance to the functionality of the reaction center. First, pump−probe anisotropy data obtained after excitation of $P \rightarrow P_{y-}$ yield the first room-temperature characterization of the P_{y+} upper excitonic state of the special pair. This characterization is based on a series of wavelength-resolved anisotropy measurements detected for varying time delays after optical excitation into the P_{y-} band. The determination of temporal, spectral, and polarization properties of all the contributing spectral entities allowed the deconvolution of the P_{y+} spectrum from the overlapping $B \rightarrow B^*$ and $P \rightarrow P_{y-}$ transitions. The results indicate that P_{y+} absorbs at 825 nm and has a transition dipole moment oriented approximately 70° from the P_{y-} transition. The energetic splitting of the two excitonic states is also seen in time domain anisotropy measurements where the two levels are coherently excited. In this case, the anisotropy oscillates with a frequency of 593 cm^{-1} corresponding to the frequency splitting between the two excitonic levels.[46,47] This frequency difference places the upper excitonic state at 823 nm, in good agreement with the spectrally resolved anisotropy results. The dipole moment orientation is in agreement with the low-temperature results from Breton,[15] although the transition energy is significantly lower. The observed spectrum, polarization, and magnitude of P_{y+} could not be modeled by simple excitonic theory where only coupling between the special pair cofactors is considered. The energetics and polarization of P_{y+} are reproduced by allowing for a significant asymmetry in the energies of P_L and P_M, but the magnitude is not captured. The failure of these models implies that a "supermolecular" approach to the electronic characteristics of the reaction center is necessary to reproduce the spectral properties of the special pair excitonic levels.

Second, internal conversion between the P_{y+} and P_{y-} excitonic states of the special pair is found to be rapid, occurring with a 65 fs time constant. This rapid internal conversion rate, as well as time- and wavelength-resolved anisotropy results indicate that the two excitonic states of the special pair are strongly coupled and significant electronic mixing is present.

Third, the Stokes shift of P_{y-} is found to occur with a 50 fs time constant, with both the ground-state bleach and stimulated emission signals strongly modulated by both low- and high-frequency coherent oscillations. To date, this is the most accurate measurement of the time scale for Stokes shift dynamics of the special pair. Vibrational dephasing dynamics of the many impulsively prepared vibrational modes were obtained. Low-frequency modes decayed within a few hundred femtoseconds, while the high-frequency oscillations, most notably at 730 cm^{-1}, exhibit dephasing times on the order of a few picoseconds. The Stokes shift dynamics observed in association with the special pair transition are, therefore, thought to be dominantly the result of a protein dielectric (i.e., solvation) response to the generation of the internal charge-separated state $P^{\pm}$. This electronic configuration is thought to precede the subsequent electron-transfer process via the B and H chromophores.

The overall excitation-transfer dynamics observed upon optical excitation of the accessory bacteriochlorophyll, which reflect both ground-state recovery and excited-state dynamics, may be modeled with a two-step energy-transfer mechanism where P_{y+} serves as an intermediate between B and P_{y-}. Within this model, the $B-P_{y+}$ step occurs with a time constant of 120 fs while the $P_{y+} \rightarrow P_{y-}$ internal conversion step has a 65 fs characteristic time. The 120 fs time constant for the first step is established by monitoring the recovery of ground-state bleach

from B, which occurs (within this model) concurrently with energy transfer from B to any other state. However, the experimental data indicate that significant excited-state evolution occurs that is not accompanied by ground-state bleach recovery. This excited-state evolution can be viewed as coherent dynamics involving coupled states of mostly B* and P_{y+} character. The electronic dephasing times of excited energy levels within the reaction center are found to range from 35 fs for $P_{y+}-P_{y-}$ coherence to 80 fs for H*−B* coherence. The observed excited-state coherence times are sufficient to allow for coherent energy-transfer mechanisms within the reaction center and clearly support a supermolecular interpretation of the electronic structure.

Acknowledgment. We thank Professors Steve Boxer, Robin Hochstrasser, and David Jonas for their comments. Gilad Haran is also acknowledged for helpful discussions about anisotropy and electronic coupling. We acknowledge the financial support of the National Institutes of Health (GM57768), the University of Pennsylvania Regional Laser Biotechnology Laboratory (NIH Facility), and Prof. Robin Hochstrasser for partial financial support of this research. C.C.M. and P.L.D. acknowledge the financial support of National Institutes of Health (GM41048). N.F.S. is a recipient of a David and Lucile Packard Foundation Fellowship, a Beckman Young Investigator Award, a National Science Foundation National Young Investigator Award (CHE-9357424), a Camile Dreyfus Teacher Scholar Award and an Alfred P. Sloan fellowship.

Note Added in Proof

After the initial submission of this manuscript, we became aware of a very relevant publication that provided a thorough investigation of energy transfer dynamics within the photosynthetic reaction center of *Rhodobacter sphaeroides* at both room temperature and at 15 K (M. H. Vos, J. Breton, and J-L Martin. *J. Phys. Chem. B*, **1997**, 101, 9820−9832). Two of their important findings were that energy transfer from B* to P_{y-} occurs via a two step mechanism involving P_{y+} as an intermediate and that B and P_{y+} can be coherently excited. Both of these results are in good agreement with the results of the present paper. With respect to the timescales of energy transfer, Vos et al. determined that the second step of this energy transfer, i.e. internal conversion within P*, occurs on a 50−100 fs timescale. This finding is also in good agreement with the results presented here of a 65 fs time constant. Furthermore, the observation by Vos et al. that B and P_{y+} can be coherently excited is supportive of our finding that the first step in energy transfer from B to P_{y+} involves coherent processes between strongly coupled states. Together, these publications provide convincing proof of coherent energy transfer mechanisms being active in the reaction center. The present paper goes beyond the work of Vos et al. by providing detailed information about the spectral and dynamical characteristics of P_{y+}, the Stokes shift dynamics of P_{y-}, and bringing additional clarity to the rapid dynamics prior to charge separation in these systems.

References and Notes

(1) Ermler, U.; Fritzsch, G.; Buchanan, S.; Michel, H. *Structure* **1994**, *2*, 925−936.

(2) Allen, J. P.; Feher, G.; Yeates, T. O.; Komiya, H.; Rees, D. C. *Proc. Natl. Acad. Sci. U.S.A.* **1987**, *84*, 5730−5734.

(3) Yeates, T. O.; Komiya, H.; Rees, D. C.; Allen, J. P.; Feher, G. *Proc. Natl. Acad. Sci. U.S.A.* **1987**, *84*, 6438−6442.

(4) Komiya, H.; Yeates, T. O.; Reees, D. C.; Allen, J. P.; Feher, G. *Proceed. Natl. Acad. Sci. U.S.A.* **1988**, *85*, 9012.

(5) Kellog, E. C.; Kolaczkowski, S.; Waseliewski, M. R.; Tiede, D. *Photosynth. Res.* **1989**, *72*, 47.

(6) Fleming, G. R.; van Grondelle, R. *Phys. Today* **1994**, 48−55.

(7) Chan, C. K.; DiMagno, T. J.; Chen, L. X. Q.; Norris, J. R.; Fleming, G. R. *Proc. Natl. Acad. Sci. U.S.A.* **1991**, *88*, 11202.

(8) Schmidt, S.; Arlt, T.; Hamm, P.; Huber, H.; Nagale, T.; Wachtveitl, J.; Meyer, M.; Scheer, H.; Zinth, W. *Chem. Phys. Lett.* **1994**, *223*, 116−120.

(9) Marchi, M.; Gehlen, J. N.; Chandler, D.; Newton, M. *J. Am. Chem. Soc.* **1993**, *115*, 4178−4190.

(10) Cory, M. G.; Zerner, M. C. *J. Am. Chem. Soc.* **1996**, *118*, 4148−4151.

(11) Thompson; Zerner, M. C. *J. Am. Chem. Soc.* **1991**, *113*, 6210.

(12) Alden, R. G.; Parson, W. W.; Chu, Z. T.; Warshel, A. *J. Am. Chem. Soc.* **1995**, *117*, 12284−12298.

(13) Scherer, P. O. J.; Scharnagl, C.; Fischer, S. F. *Chem. Phys.* **1995**, *197*, 33−341.

(14) Won, Y.; Friesner, R. A. *J. Phys. Chem.* **1988**, *92*, 2208−2214.

(15) Breton, J. *Biochim. Biophys. Acta* **1985**, *810*, 235−245.

(16) Tang, D.; Johnson, S. G.; Jankowiak, R.; Hayes, J. M.; Small, G. J.; Tiede, D. M.. In *Perspectives in Photosynthesis*; Jortner, J., Pullman, B., Eds.; Kluwer Academic Publisher: The Netherlands, 1990; p 99.

(17) Reddy, J. R. S.; Kolaczkowski, S. V.; Small, G. J. *J. Phys. Chem.* **1995**, *97*, 6934.

(18) Breton, J.; Martin, J.-L.; Fleming, G. R.; Lambry, J.-C. *Biochemistry* **1988**, *27*, 8276−8284.

(19) Haran, G.; Wynne, K.; Moser, C. C.; Dutton, P. L.; Hochstrasser, R. *J. Phys. Chem.* **1996**, *100*, 5562.

(20) Jonas, D. M.; Lang, M. J.; Nagasawa, Y.; Joo, T.; Fleming, G. R. *J. Phys. Chem.* **1996**, *100*, 12660−12673.

(21) Förster, T. Delocalized Excitation and Excitation Transfer. In *Modern Quantum Chemistry: Instanbul Lectures*; Sinanoglu, O., Ed.; Academic Press: New York, 1965; Vol. 3; pp 93−137.

(22) Jean, J. M.; Chan, C.-K.; Fleming, G. R. *Isr. J. Chem.* **1988**, *28*, 169−175.

(23) Stanley, R. J.; King, B.; Boxer, S. G. *J. Phys. Chem.* **1996**, *100*, 12052−12059.

(24) van Brederode, M. E.; Jones, M. R.; van Grondelle, R. *Chem. Phys. Lett.* **1997**, *268*, 143−149.

(25) van Brederode, M. E.; Jones, M. R.; van Mourik, F.; van Stokkum, I. H. M.; van Grondelle, R. *Biochemistry* **1997**, *36*, 6855−6861.

(26) van Grondelle, R. Private Communication.

(27) Arnett, D. C.; Book, L.; Moser, C. C.; Dutton, P. L.; Scherer, N. F. *J. Phys. Chem.*, submitted.

(28) Arnett, D. C.; Vöhringer, P.; Scherer, N. F. *J. Am. Chem. Soc.* **1995**, *117*, 12262−12272.

(29) Liau, Y-H.; Arnett, D. C.; Scherer, N. F. *Opt. Letters*, submitted (1999).

(30) Sweetser, J. N.; Fittinghoff, D. N.; Trebino, R. *Opt. Lett.* **1997**, *22*, 519−521.

(31) DeLong, K. W.; Trebino, R.; Kane, D. *J. Opt. Soc. Am. B.* **1994**, *11*, 1595.

(32) Vöhringer, P.; Westervelt, R. A.; Yang, T.-S.; Arnett, D. C.; Feldstein, M. J.; Scherer, N. F. *J. Raman Spectrosc.* **1995**, *26*, 535−551.

(33) Scherer, N. F.; Jonas, D. M.; Fleming, G. R. *J. Chem. Phys.* **1993**, *99*, 153−168.

(34) Clayton, R. K.; Wang, R. T. *Methods Enzymol.* **1971**, *23*, 696.

(35) Siegman, A. *Lasers*; University Science Books: Mill Valley CA, 1986.

(36) Jia, Y.; DiMagno, T. J.; Chan, C.-K.; Wang, Z.; Du, M.; Hanson, D. K.; Schiffer, M.; Norris, J. R.; Fleming, G. R. *J. Phys. Chem.* **1993**, *97*, 13180−13191.

(37) Jia, Y.; Jonas, D. M.; Joo, T.; Nagasawa, Y.; Lang, M. J.; Fleming, G. R. *J. Phys. Chem.* **1995**, *99*, 6263−6266.

(38) Vos, M. H.; Lambry, J.-C.; Robles, S. J.; Youvan, D. C.; Breton, J.; Martin, J.-L. *Proc. Natl. Acad. Sci. U.S.A.* **1992**, *89*, 613−617.

(39) Kirmaier, C.; Holten, D. *Photosynth. Res.* **1987**, *13*, 225−260.

(40) Du, M.; Rosenthal, S. J.; Xie, X.; Dimagno, T. J.; Schmidt, M.; Hanson, D. K.; Schiffer, M.; Norris, J. R.; Fleming, G. R. *Proc. Natl. Acad. Sci. U.S.A.* **1992**, *89*, 8517−8521.

(41) Vos, M. H.; Jones, M. R.; Hunter, C. N.; Breton, J.; Martin, J.-L. *Proc. Natl. Acad. Sci. U.S.A.* **1994**, *91*, 12701−12805.

(42) Vos, M. H.; Jones, M. R.; Hunter, C. N.; Breton, J.; Lambry, J. C.; Martin, J.-L. *Biochemistry* **1994**, *33*, 6750−6757.

(43) Vos, M. H.; Rappaport, F.; Lambry, J.-C.; Breton, J.; Martin, J.-L. *Nature* **1993**, *363*, 320−325.

(44) Stanley, R. J.; Boxer, S. G. *J. Phys. Chem.* **1995**, *99*, 859−863.

(45) Steffen, M. A.; Lao, K.; Boxer, S. G. *Science* **1994**, *264*, 810−816.

(46) Wynne, K.; Hochstrasser, R. M. *Chem. Phys.* **1993**, *171*, 179−188.

(47) Wynne, K.; Hochstrasser, R. M. *J. Raman Spectrosc.* **1995**, *26*, 561−569.

(48) Nagarajan, V.; Alden, R. G.; Williams, J. C.; Parson, W. W. *Proc. Natl. Acad. Sci. U.S.A.* **1996**, *93*, 13774−13779.
(49) Savikhin, S.; Buck, D. R.; Struve, W. S. *J. Chem. Phys.*, in press.
(50) Arnett, D.; Kumble, R.; Vischers, R.; Hochstrasser, R. M.; Scherer, N. F. *J. Phys. Chem.*, to be submitted.
(51) Steinfeld, J. I.; Francisco, J. S.; Hase, W. L. *Chemical Kinetics and Dynamics*; Prentice Hall: Englewood Cliffs, California, 1989.
(52) Becker, M.; Nagarajan, V.; Parson, W. *J. Am. Chem. Soc.* **1991**, *113*, 6840.
(53) Connolly, J. S.; Samuel, E. B.; Janzen, A. F. *Photochem. Photobiol.* **1982**, *36*, 565.
(54) Mar, T.; Gingras, G. *Biochim. Biophys. Acta* **1984**, *764*, 283−294.
(55) Wang, Z.; Pearlstein, R. M.; Jia, Y.; Fleming, G. R.; Morris, J. R. *Chem. Phys.* **1993**, *176*, 421−425.
(56) Scherer, P. O. J.; Fischer, S. F.; Lancaster, C. R. D.; Fritzsch, G.; Schmidt, S.; Arlt, T.; Dressler, K.; Zinth, W. *Chem. Phys.* **1994**, *223*, 110−115.
(57) Xu, D.; Schulten, K. *Chem. Phys.* **1994**, *182*, 91−117.
(58) Mukamel, S. *Nonlinear Optical Spectroscopy*; Oxford: Oxford, 1995.
(59) Joo, T.; Jia, Y.; Yu, J.-Y.; Lang, M. J.; Fleming, G. R. *J. Chem. Phys.* **1996**, *104*, 6089.
(60) Yan, Y. J.; Mukamel, S. *Phys. Rev. A.* **1990**, *41*, 6485.
(61) Bagchi, B.; Oxtoby, D. W.; Fleming, G. R. *Chem. Phys.* **1984**, *86*, 257.
(62) Rosenthal, S. J.; Xie, X. L.; Du, M.; Fleming, G. R. *J. Chem. Phys.* **1991**, *95*, 4715.
(63) de Boeij, W. P.; Pshenichnikov, M. S.; Wiersma, D. A. *J. Phys. Chem.* **1996**, *100*, 11806−11823.
(64) Cherepy, N. J.; Shreve, A. P.; Moore, L. J.; Franzen, S.; Boxer, S. G.; Mathies, R. A. *J. Phys. Chem.* **1994**, *98*, 6023−6029.
(65) Arnett, D. C.; Moser, C. C.; Dutton, P. L.; Scherer, N. F. *J. Phys. Chem.*, in preparation.
(66) Small, G. J. *Chem. Phys.* **1995**, *197*, 239−257.
(67) Joo, T.; Jia, Y.; Yu, J.-Y.; Jonas, D. M.; Fleming, G. R. *J. Phys. Chem.* **1996**, *100*, 2399−2409.
(68) Lyle, P. A.; Kolaczkowski, S. V.; Small, G. J. *J. Phys. Chem.* **1993**, *97*, 6924−6933.
(69) Raja, N.; Reddy, S.; Kolaczkowski, S. V.; Small, G. J. *J. Phys. Chem.* **1993**, *97*, 6934−6940.
(70) Meech, S. R.; Hoff, A. J.; Wiersma, D. A. *Chem. Phys. Lett.* **1985**, *121*, 287−292.
(71) Boxer, S. G.; Lockhardt, D. J.; Middendorf, T. R. *Chem. Phys. Lett.* **1986**, *123*, 476.
(72) Souaille, M.; Marchi, M. *J. Am. Chem. Soc.* **1997**, *119*, 3948−3958.
(73) Riter, R. E.; Edington, M. D.; Beck, W. F. *J. Phys. Chem. B* **1997**, *101*, 2366−2371.
(74) Kumble, R.; Palese, S.; Visschers, R. W.; Dutton, P. L.; Hochstrasser, R. M. *Chem. Phys. Lett.* **1996**, *261*, 396−404.
(75) Vulto, S. I. E.; Streltsov, A. M.; Shkuropatov, A. Y.; Shuvalov, V. A.; Aartsma, T. J. *J. Phys. Chem. B* **1997**, *101*, 7249−7255.
(76) Arnett, D. C.; Moser, C. C.; Dutton, P. L.; Scherer, N. F. In *Ultrafast Phenomena X*, Springer Series in Chemical Physics; P. F. Barbara, Ed.; **1996**, *62*, 334−335.